BIOCHEMISTRY
including biophysical chemistry & molecular biology

Article

pubs.acs.org/biochemistry

Mutation of Lysine 317 in the D2 Subunit of Photosystem II Alters Chloride Binding and Proton Transport

Ravi Pokhrel,[†] Rachel J. Service,[‡,§] Richard J. Debus,*[,‡] and Gary W. Brudvig*[,†]

[†]Department of Chemistry, Yale University, New Haven, Connecticut 06520-8107, United States
[‡]Department of Biochemistry, University of California, Riverside, California 92521, United States

Supporting Information

ABSTRACT: The role of chloride in photosystem II (PSII) is unclear. Using structural information from PSII and a careful comparison with other chloride-activated enzymes, we proposed a role for chloride at the D2-K317 site in PSII [Pokhrel, R., et al. (2011) *Biochemistry 50*, 2725−2734]. To probe the role of chloride at this site, the D2-K317R, D2-K317A, D2-K317Q, and D2-K317E mutations were created in the cyanobacterium *Synechocystis* sp. PCC 6803. Purified PSII from the mutants was probed with Fourier transform infrared difference spectroscopy, demonstrating that compared to PSII from wild-type *Synechocystis*, PSII from all four mutants exhibit changes in the conformations of the polypeptide backbone and carboxylate groups. However, D2-K317R PSII exhibits minor changes, whereas D2-K317A, D2-K317Q, and D2-K317E PSII exhibit more substantial changes in polypeptide conformations. Steady-state oxygen-evolution measurements of purified PSII core complexes show that the oxygen-evolution activity of D2-K317A is independent of chloride. This is consistent with the loss of the chloride requirement when the charged K residue is replaced with an uncharged residue that no longer binds to an essential carboxylate (D1-D61) in the absence of chloride, analogous to observations in other chloride-activated enzymes. In contrast, the oxygen-evolution activity of D2-K317R is sensitive to the chloride concentration in the assay buffer; the effective K_D for chloride binding is higher in D2-K317R than in wild-type PSII, possibly because of a less optimal binding site in the mutant. The S_2 states of wild-type, D2-K317A, and D2-K317R PSII were probed using electron paramagnetic resonance spectroscopy. A $g = 2$ multiline signal, similar to the wild-type signal, was observed for D2-K317A and D2-K317R. However, a $g = 4$ signal was also observed for D2-K317R. Measurements of flash-dependent O_2 yields showed that D2-K317A and D2-K317R have a higher miss factor than wild-type PSII. The oxygen-release kinetics of D2-K317A and D2-K317R were slower than those of the wild type, in the following order: D2-K317A < D2-K317R < wild type. These results collectively suggest that proton transfer is inefficient in D2-K317A and D2-K317R, thereby giving rise to a higher miss factor and slower oxygen-release kinetics.

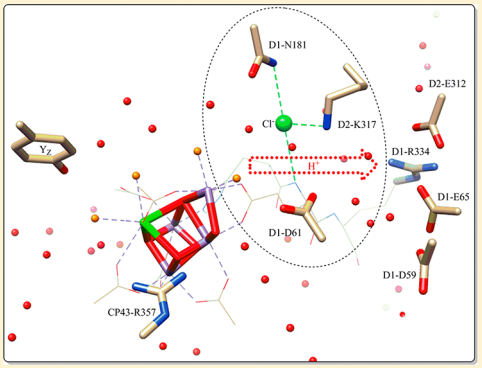

Photosystem II (PSII) catalyzes light-driven water oxidation as part of oxygenic photosynthesis. The active site for water oxidation is the O_2-evolving complex (OEC), a Mn_4CaO_5 cluster buried in the protein but with substantial access to water and other small molecules.[1] The OEC advances through a series of light-driven oxidations during catalysis. The oxidation states of the OEC are known as the S states, or the storage states.[2] The most reduced S_0 state is progressively oxidized to the most oxidized S_4 state using the redox energy generated by photochemistry. When an exciton reaches the reaction center pigments of PSII, P_{680}, the resulting photoexcited RC pigments, P_{680}*, trigger a series of electron-transfer events that result in an ultrafast charge separation across the membrane bilayer.[3] A stable charge separation that forms $P_{680}^{\bullet+}$ and $Q_A^{\bullet-}$, a membrane-bound semiquinone radical, drives the oxidation of the OEC. $P_{680}^{\bullet+}$ oxidizes the OEC via a redox-active tyrosine residue, Y_Z, while $Q_A^{\bullet-}$ transfers the electron to the terminal electron acceptor in PSII, a plastoquinone molecule, Q_B.

When water is oxidized at the OEC using the energy harnessed from sunlight, O_2 is produced as a byproduct. The rate of O_2 evolution under illumination is commonly used as a measure of activity of the OEC. It has been known for many decades that Cl^- is an essential cofactor for the maximal rate of O_2 evolution.[4−6] A $^{36}Cl^-$ labeling study using PSII isolated from spinach shows that there is one high-affinity Cl^- bound per PSII that is important for activity.[7] The K_D of Cl^- binding in PSII membranes isolated from spinach varies in the presence and absence of the PsbP and PsbQ extrinsic subunits, with a much tighter binding of Cl^- observed in the presence of these subunits.[8,9] The binding affinity of Cl^- changes with different Cl^- depletion procedures, and is correlated to the loss of the extrinsic subunits. Several other monovalent anions and amines compete for the Cl^- site in PSII, and some of these competing

Received: December 24, 2012
Revised: June 16, 2013
Published: June 20, 2013

 © 2013 American Chemical Society dx.doi.org/10.1021/bi301700u | *Biochemistry* 2013, 52, 4758−4773

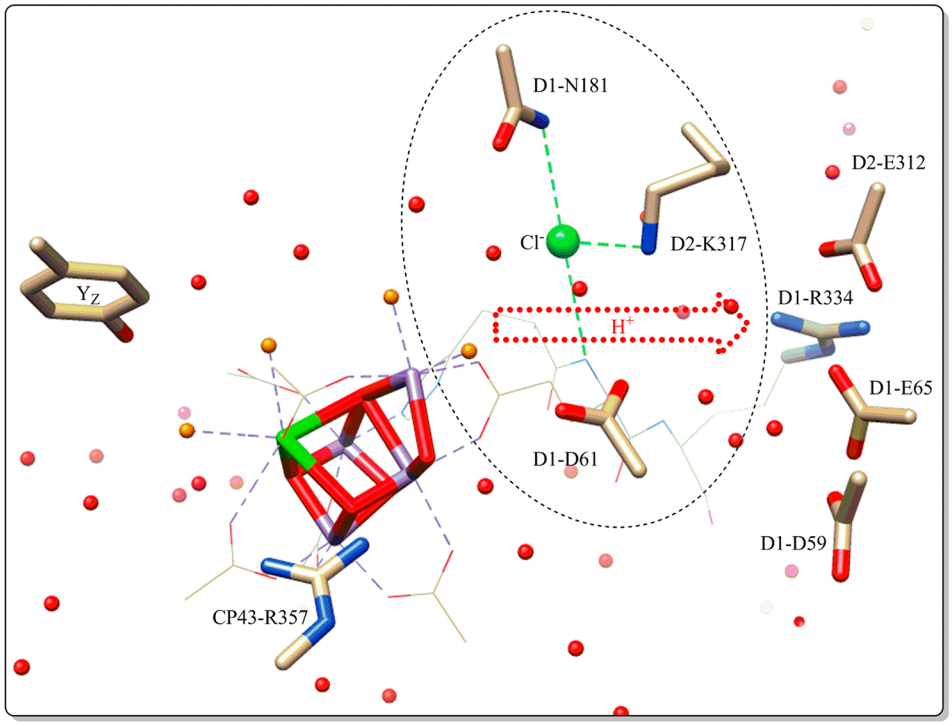

Figure 1. D2-K317 Cl^--binding site shown in relation to the D1-D61 residue, CP43-R357 residue, other nearby ionizable residues, the OEC, OEC-bound water molecules (orange), some other nearby water molecules (red), and the Y_Z residue. All amino acid ligands to the OEC are shown as lines (not labeled). The dashed oval encloses the triad of D1-D61, D2-K317, and Cl^- that was investigated, and the dotted red arrow represents the postulated proton exit pathway from the OEC to the lumen.

monovalent anions support activity.[10−14] The ability to support maximal rates of O_2 evolution decreases in the following order: $Cl^- > Br^- \gg NO_3^- > NO_2^- > I^-$.[15]

Flash-based UV−visible spectrophotometric measurements of PSII show that Cl^- is required for only the $S_2 \rightarrow S_3$ and $S_3 \rightarrow S_0$ transitions.[16] The $S_1 \rightarrow S_2$ transition is not blocked upon Cl^- depletion. However, the S_2-minus-S_1 FTIR difference spectra of PSII membranes in the presence and absence of Cl^- show clear differences in the amide I, amide II, and carboxylate vibrational modes.[17] Addition of Cl^- to the Cl^--depleted membranes shows reversibility of the FTIR spectral features.[17] This result indicates reversible structural differences of the protein backbone and one or more carboxylate residues in the presence and absence of Cl^-. Further support for structural changes around the OEC upon removal of Cl^- comes from the S_2-state EPR spectra of PSII membranes. The S_2-state $g = 4.1$ EPR signal appears in lieu of the S_2-state $g = 2$ multiline signal in Cl^--depleted PSII membranes.[18,19] Interestingly, addition of Cl^- to the Cl^--depleted PSII membranes in the dark shifts the equilibrium back to the S_2-state multiline signal.[18] The effect of Cl^- binding on the magnetic properties of the OEC clearly indicates structural communication between the Cl^- site and the OEC. An equilibrium favoring the centers giving rise to the $g = 4.1$ signal over the centers giving rise to the $g = 2$ multiline signal is also observed when Cl^- is substituted with amines, CH_3COO^-, N_3^-, I^-, and F^-.[10,11,20,21] The $g = 4.1$ S_2-state EPR signal has not normally been observed in "Cl^--depleted" cyanobacterial PSII. However, a $g = 4$ S_2-state EPR signal was identified in cyanobacterial PSII upon substitution of Cl^- with I^-, similar to what is observed in PSII isolated from spinach.[22] A $g = 4.1$ signal has also been observed in Sr-substituted PSII from *Synechocystis* sp. PCC 6803.[23] A tighter binding of Cl^- in cyanobacterial PSII, and hence more difficulty in removing Cl^- from its binding site, could explain the lack of observation of the $g = 4.1$ S_2-state EPR signal in "Cl^--depleted" PSII cores from cyanobacteria.

Many proposals for the mechanism of Cl^- activation have been advanced during the investigation of the role of Cl^- in PSII. Most of the earlier proposals involved Cl^- as a ligand to Ca or Mn in the OEC.[14,24,25] However, Ono suggested that Cl^- was structurally coupled to the OEC but not directly bound to the OEC.[17,26] There were proposals for a role in regulating the redox potential of the OEC and in substrate water activation.[27,28] Andréasson has argued that Cl^- is not required for O_2 evolution and that the Cl^- effect is an artifact of harsh Cl^- depletion procedures.[29] Moreover, Andréasson also suggested that the possible role of Cl^- could be to facilitate the exit of a proton from the OEC to the lumen. More recently, EXAFS and crystallographic studies have shown that Cl^- is not a ligand to the OEC.[1,30−33] Interestingly, two Cl^- sites, both approximately 6−7 Å from the OEC, have been identified in recent crystal structures. One Cl^- ion is ion paired to the D2-K317 residue in addition to being hydrogen bonded to a backbone amide NH group and the D1-N181 side chain, as shown in Figure 1, whereas the other Cl^- ion is stabilized by hydrogen bonding interactions to only two backbone amide NH groups. When more structural details about the location of Cl^- binding became available, it was proposed that the roles of Cl^- are to facilitate access of substrate waters to the OEC, to aid in the removal of protons from the OEC, and to maintain the coordination structure of the OEC.[31,33]

By analyzing the Cl^--binding sites in other Cl^--activated enzymes, Brudvig and co-workers proposed a novel mechanism by which PSII is activated by Cl^- bound to the D2-K317 site.[4] In their proposal, a salt bridge forms between D2-K317 and D1-D61 upon removal of Cl^- from the D2-K317 site. A shift in

dx.doi.org/10.1021/bi301700u | *Biochemistry* 2013, 52, 4758−4773

the pK_a of the D1-D61 residue when it is engaged in the salt bridge makes it an inefficient proton acceptor during the S-state cycle. Hence, the role of Cl^- at the D2-K317 site was proposed to be in tuning the pK_a of the D1-D61 residue and in positioning the D1-D61 residue for efficient removal of a proton from the OEC.[4] Molecular dynamics (MD) simulations and multiconformer continuum electrostatics (MCCE) calculations confirm that a salt bridge can, indeed, be formed between D2-K317 and D1-D61 when Cl^- is removed from the D2-K317 binding site.[34] Furthermore, these calculations indicate that D1-D61 moves away from the OEC on forming a salt bridge with D2-K317, which disrupts the hydrogen-bonding network that is postulated to be required for proton transport.[34]

Most biochemical studies probing the role of Cl^- in PSII have been conducted using PSII isolated from spinach, whereas all the structural information about the Cl^--binding sites is based on PSII isolated from cyanobacteria. However, several mutagenesis studies of *Synechocystis* PSII have shown an increase in the stringency of the chloride requirement upon mutations in the CP43 or CP47 subunit.[35−41]

In this study, we have characterized the effect of point mutations at the D2-K317 residue to improve our understanding of the role of Cl^- bound at the D2-K317 site in PSII isolated from *Synechocystis* sp. PCC 6803. We introduced four point mutations at the D2-K317 residue: D2-K317A, D2-K317Q, D2-K317R, and D2-K317E. We found that the steady-state oxygen-evolution activity of D2-K317A PSII was independent of Cl^-, whereas the activity of D2-K317R PSII was dependent on Cl^-, with a larger effective K_D for Cl^- binding than for the wild type. FTIR measurements on PSII isolated from the D2-K317 mutants showed differences from the wild type, suggesting differences in the conformations of the polypeptide backbone and some carboxylates. The S_2 state of the OEC of D2-K317A and D2-K317R was studied using EPR spectroscopy. Flash-induced O_2 yield patterns and O_2-release kinetics were also measured for WT, D2-K317A, and D2-K317R PSII.

MATERIALS AND METHODS

Construction of Site-Directed Mutants and Propagation of Cultures. The D2-K317R, D2-K317A, D2-K317Q, and D2-K317E mutations were constructed in the *psbD-1* gene of *Synechocystis* sp. PCC 6803[42] and transformed into a host strain of *Synechocystis* that lacked both *psbD* genes and contained a hexahistidine tag (His tag) fused to the C-terminus of CP47.[43] Single colonies were selected for their ability to grow on solid media containing 5 μg/mL kanamycin monosulfate and 20 μg/mL gentamycin sulfate.[43] The solid media contained 5 mM glucose and 10 μM DCMU. The DCMU and antibiotics were omitted from liquid cultures. Large-scale liquid cultures (each consisting of three 7 L cultures held in glass carboys) were inoculated from small-scale liquid cultures and propagated as described previously.[44] For growth in "chloride-free" medium, calcium sulfate and manganese sulfate replaced their respective chloride salts and cells were propagated in polycarbonate flasks to prevent leaching of chloride from glass.[38] The chloride concentration in the growth media was determined with a chloride specific combination electrode (model 96-17B, Orion Research Inc., Boston, MA) after the pH of the medium had been adjusted from 8.0 to 6.0 with nitric acid. For the purification of PSII core complexes that had been uniformly labeled with ^{15}N, liquid cultures were propagated in the presence of 10 mM $Na^{15}NO_3$ as the sole nitrogen source [98% ^{15}N enrichment (Cambridge Isotope Laboratories, Andover, MA)].[45,46] To verify the integrity of the mutant cultures that were harvested for the purification of PSII core complexes, we set aside an aliquot of each culture and determined the sequence of the region of *psbD-1* that contains the D2-K317 codon after polymerase chain reaction amplification of genomic DNA.[47] No trace of the wild-type codon was detected in any of the mutant cultures.

Purification of PSII Core Complexes. Oxygen-evolving PSII core complexes were purified under dim green light at 4 °C with a Ni-NTA superflow affinity resin (Qiagen, Valencia, CA) as described previously.[23] The purified PSII core complexes [in 1.2 M betaine, 10% (v/v) glycerol, 50 mM MES-NaOH (pH 6.0), 20 mM $CaCl_2$, 5 mM $MgCl_2$, 50 mM histidine, 1 mM EDTA, and 0.03% (w/v) *n*-dodecyl β-D-maltoside] were concentrated to ∼1.0 mg of Chl/mL by ultrafiltration, frozen in liquid N_2, and stored at −80 °C.

Gel Electrophoresis. Sodium dodecyl sulfate−polyacrylamide gel electrophoresis (SDS−PAGE) was performed with a gel containing a 16 to 24% acrylamide gradient and 6 M urea.[48] Samples (8 μg of Chl per lane) were extracted with methanol and ethyl ether as described previously[48] to remove membrane lipids and pigments. Bands corresponding to the CP43, D2, psbV, psbQ, and psbU proteins were identified by matrix-assisted laser desorption ionization (MALDI) mass spectrometry of peptides generated by in-gel digestion of bands with trypsin.[49] Bands corresponding to the CP47, D1, and psbO proteins were identified by comparison with gels run under similar conditions[50,51] and by the loss of psbO and other extrinsic proteins after treatment with 1 M $CaCl_2$.[52]

Preparation of FTIR Samples. All manipulations were conducted under dim green light at 4 °C. Samples (50−70 μg of Chl *a*) were exchanged into FTIR analysis buffer [40 mM sucrose, 10 mM MES-NaOH (pH 6.0), 5 mM $CaCl_2$, 5 mM NaCl, and 0.06% (w/v) *n*-dodecyl β-D-maltoside[45,53]] by being passed through a centrifugal gel filtration column at 27*g*.[54] They were then concentrated to 3−5 mg of Chl/mL with Amicon Ultra 0.5 mL 100K centrifugal filters (Millipore Corp., Billerica, MA). Concentrated samples (6−8 μL in volume) were mixed with 1/10 volume of fresh 100 mM potassium ferricyanide (dissolved in water), spread to a diameter of ∼13 mm in the center of a 25 mm × 2 mm diameter BaF_2 window, and then dried lightly (until tacky) under a stream of dry nitrogen gas. To maintain the sample at 99% relative humidity in the FTIR sample compartment, four 1 μL drops of a solution of 20% (v/v) glycerol in water were spotted around the periphery of the window, not touching the sample.[55] A second BaF_2 window was placed over the first, with a 23 mm × 1 mm nitrile O-ring acting as a spacer. The sample assembly was sealed into an aluminum cell, loaded into a water-jacketed aluminum holder in the FTIR sample compartment, and allowed to equilibrate in the dark for 2 h. The sample was kept at a constant temperature of 0 °C by circulating a cold solution of 50% (v/v) ethylene glycol in water through the sample cell holder. Sample concentrations were adjusted so that the absolute absorbance of the amide I band at 1657 cm^{-1} was 0.7−1.3.

FTIR Spectra. Midfrequency FTIR spectra were recorded with a Bruker Vertex 70 spectrometer (Bruker Optics, Billerica, MA) that was equipped with a KBr beam splitter and a preamplified, midrange D317 photovoltaic MCT detector (Kolmar Technologies, Inc., Newburyport, MA). Long-pass 2.4 μm cutoff filters (Andover Corp., Salem, NH) were

mounted on both sides of the sample compartment to prevent the interferometer's coaxial helium−neon laser from illuminating the sample and to protect the MCT detector from scattered actinic illumination. Double-sided forward−backward interferograms were recorded with a scanner velocity of 120 kHz. For the calculation of Fourier transforms, a Blackman-Harris three-term apodization function and a zero-fill factor of 2 were employed. The spectral resolution for all spectra was 4 cm^{-1}. Actinic illumination consisted of flashes (~20 mJ/flash, ~7 ns full width at half-maximum) provided by a frequency-doubled Q-switched Nd:YAG laser [BRIO (Quantel USA, Bozeman, MT)]. Flash excitation was controlled from the Vertex 70 OPUS interface. The Nd:YAG laser was programmed to deliver a single Q-switched flash during a 20 Hz flashlamp repetition series to ensure the uniformity of the laser light intensity. For each sample, after dark adaptation, six successive flashes were applied with an interval of 13 s between each (no preflashes were applied). Two single-beam spectra were recorded before the first flash, and one single-beam spectrum was recorded starting 0.33 s after the first and subsequent flashes (each single-beam spectrum consisted of 100 scans). The 0.33 s delay was incorporated to allow for the oxidation of Q_A^- by the ferricyanide. To obtain difference spectra corresponding to successive S-state transitions, the single-beam spectrum that was recorded after the *n*th flash was divided by the single-beam spectrum that was recorded immediately before the *n*th flash and the ratio was converted to units of absorption. To estimate the background noise level, the second preflash single-beam spectrum was divided by the first and the ratio was converted to units of absorption. The sample was adapted to the dark for 30 min, and then the cycle was repeated. The cycle was repeated 14−16 times for each sample, and the difference spectra recorded with several samples were averaged.

Cl^- Removal and Oxygen-Evolution Assays. Purified PSII from wild type, D2-K317A, and D2-K317R were dialyzed against "chloride-free" buffer in the dark for 20 h. The "chloride-free" buffer contained 1 M sucrose, 5 mM Ca^{2+} [using $Ca(OH)_2$], and MES (pH 7.5). Fifteen grams of anion exchange AG1-X8 resin (Bio-Rad Laboratories) was also added per liter of dialysis buffer to remove background chloride. The pH was adjusted to 7.5 with MES after the addition of the anion exchange resin. Oxygen-evolution assays were performed using aliquots of the dialyzed protein samples. The "chloride-free" 1 M sucrose, 5 mM Ca^{2+}, MES (pH 7.5) buffer was also used for oxygen-evolution assays. Appropriate volumes of sodium chloride were added from a stock solution to obtain the desired chloride concentration in the assay buffers. Oxygen evolution was monitored with a Clark-type electrode, and the oxygen assay chamber was maintained at 25 °C using a temperature-controlled water bath. Samples were illuminated with an Oriel 1000 W tungsten−halogen lamp. A water filter was used to avoid heating of the sample; 250 μM DCBQ and 1 mM K_3FeCN_6 were used as electron acceptors during the assays, and 10 μg of Chl was used in each assay. PSII core complexes and electron acceptors were added to the buffer in the chamber while the sample was being stirred. The light source was turned on after the sample had been mixed in the chamber for ~2 min.

Electron Paramagnetic Spectroscopy. EPR samples were prepared by concentrating purified PSII cores using Amicon Centrifugal Filter Units with a 30 kDa cutoff. EPR scans were acquired on a Bruker ELEXSYS E500 EPR spectrometer equipped with a SHQ resonator and an Oxford ESR-900 helium-flow cryostat. The S_1-state spectra were obtained in the dark using dark-adapted PSII core complexes. The S_2-state spectra were obtained after illumination of the samples in a 200 K dry ice/acetone bath for 5 min. EPR scans were performed at 6.5 K with the following instrumental parameters: microwave frequency, 9.38 GHz; modulation frequency, 100 kHz; modulation amplitude, 31 G; and microwave power, 5 mW.

Flash-Induced Oxygen Measurement. Flash-induced polarographic measurements were taken using a bare platinum electrode. The electrochemical cell was comprised of a Pt disk working electrode and a Ag ring counter electrode. The Ag ring was also used as the reference electrode. Purified PSII core complexes (9 μg of Chl) were diluted to a total volume of 1 mL using a buffer containing 20% (w/v) PEG 6000, 25 mM $CaCl_2$, 50 mM NaCl, and 50 mM MES-NaOH (pH 6.5). PSII in PEG buffer was then added to the platinum electrode. A Teflon fitting was used in the electrode to contain the solution within the Pt electrode surface. The PSII cores were preflashed with five flashes at 1 Hz and immediately centrifuged using an HS-4 swing out rotor at 4000 rpm for 15 min in the dark. After the cores pelleted on the platinum disk, the Teflon fitting was removed, and the PEG buffer was exchanged for a 2 mL volume of buffer containing 1 M sucrose, 10 mM $CaCl_2$, 200 mM NaCl, and 50 mM MES-NaOH (pH 6.50). DCBQ and K_3FeCN_6 were added to final concentrations of 500 μM and 1 mM, respectively. The electrode was polarized for 10 s before data were acquired, after which the flash sequence was initiated. For single-turnover flashes, a xenon flash lamp (#FX 249, EG&G electro-optics) triggered by a FY-712 "Lite-Pac" module (EG&G electro-optics) and a BK precision 3300 pulse generator were used in all experiments. The S-state parameters, misses and double hits, were obtained by fitting the data assuming a four-state model. For experiments conducted at 0 °C, the centrifugation steps were performed at 0 °C, and once the electrode was removed from the centrifuge, an ice/water jacket was used to maintain the temperature at 0 °C. Data for flash oxygen kinetics were obtained at a 100 μs/interval spacing.

RESULTS

Growth, Steady-State Oxygen Evolution, and Cl^- Dependence. Cells of the D2-K317R, D2-K317A, D2-K317E, and D2-K317Q mutants were photoautotrophic but grew more slowly than wild-type cells. The A_{730} doubling times for D2-K317R, D2-K317A, D2-K317E, and D2-K317Q cells under photoautotrophic conditions were approximately 19, 25, 34, and 40 h, respectively, compared to approximately 14 h for wild-type cells (see Figure S1 of the Supporting Information). The light-saturated, steady-state O_2-evolving activities of D2-K317R, D2-K317A, D2-K318E, and D2-K317Q cells in regular assay buffer were approximately 390, 460, 270, and 205 μmol of O_2 (mg of Chl)$^{-1}$ h^{-1}, respectively, compared to approximately 680 μmol of O_2 (mg of Chl)$^{-1}$ h^{-1} for wild-type cells. The light-saturated, steady-state O_2-evolving activities in regular buffer of PSII core complexes purified from D2-K317R and D2-K317A were approximately 1200−1500 μmol of O_2 (mg of Chl)$^{-1}$ h^{-1}, and the light-saturated, steady-state O_2-evolving activities in regular buffer of PSII core complexes purified from D2-K317E and D2-K317Q cells were approximately 700−900 μmol of O_2 (mg of Chl)$^{-1}$ h^{-1}, compared to approximately 2400−2800 μmol of O_2 (mg of Chl)$^{-1}$ h^{-1} for wild-type PSII. In the absence of calcium in the assay buffer, we observed a

25−45% decrease in the oxygen-evolution activity of PSII core complexes isolated from WT and the mutants. The lower activities of the purified mutated PSII core complexes compared to that of wild-type PSII suggest either that the Mn_4Ca clusters in the mutants are somewhat labile or that the efficiency of S-state turnover is lower in the mutated PSII core complexes than in WT PSII core complexes. Analysis of the polypeptide compositions of purified PSII core complexes with SDS−PAGE showed no apparent differences between the mutant and wild-type preparations: a 16 to 24% gradient acrylamide gel showed that all three extrinsic proteins, PsbO, PsbU, and PsbV, were present in the PSII core complexes isolated from the D2-K317A, -Q, -R, and -E mutants (Figure S2 of the Supporting Information). Interestingly, the D2 polypeptide migrated ∼1 kDa larger in the A and Q mutants than in the wild type and ∼2 kDa larger in the E mutant. Anomalous migration of the D2 polypeptide in D2 mutants has been reported previously.[56]

Growth rates in "chloride-free" media were tested for wild-type and D2-K317 mutant cells (Figure S1 of the Supporting Information). The growth rates for the wild type and D2-K317R in "chloride-free" media were roughly 70−80% of the growth rates in normal media, whereas the growth rate for D2-K317A in "chloride-free" media was similar to the rate in chloride sufficient media. However, D2-K317Q and D2-K317E grew in "chloride-free" media at roughly 40−50% of the growth rates in normal media. When the D2-K317Q and D2-K317E cells growing in "chloride-free" media were transferred to normal media, normal growth rates were restored.

The chloride dependence of the oxygen-evolution activities of purified PSII isolated from wild-type, D2-K317A, and D2-K317R was measured. PSII core complexes were dialyzed against "Cl^--free" buffer for 20 h to remove chloride. Other methods of chloride removal such as the high-pH treatment method and the extrinsic polypeptide removal method were not pursued to avoid harsh treatments. Because of a strong binding of Cl^- in wild-type PSII, we observed ∼80% activity in the absence of any added Cl^- in the assay buffer (Figure 2). Wild-type PSII may have a high activity even in the absence of added Cl^- because of a background Cl^- contamination of ∼50 μM chloride. However, the oxygen-evolution activity of D2-K317R PSII was more sensitive to Cl^- in the assay buffer [Figure 2; a similar observation was made by Suzuki et al.[57]]. The requirement of Cl^- for activity was conserved in the D2-K317R mutant, but the effective K_D for Cl^- binding was altered. In addition to low rates of initial oxygen production by D2-K317R PSII, the extent of oxygen evolution declined during illumination when chloride was absent from the assay media (Figure S3 of the Supporting Information). However, in the presence of Cl^-, higher rates of oxygen production were sustained over longer time periods. This indicated a loss of Cl^- during turnover in the D2-K317R mutant that led to a loss of oxygen production at the OEC. On the basis of our Cl^- titration, we estimate the effective K_D for Cl^- binding to be around 100 μM for the D2-K317R mutant. The effective K_D for wild-type PSII could not be estimated because of the background Cl^- concentrations in the assay buffer that supported significant activity even in the absence of added chloride.

In contrast to the D2-K317R mutant, the oxygen-evolution activity of D2-K317A PSII was independent of Cl^- (Figure 2). When the positively charged K residue is replaced with an uncharged A residue, there is no Cl^- binding at this site.

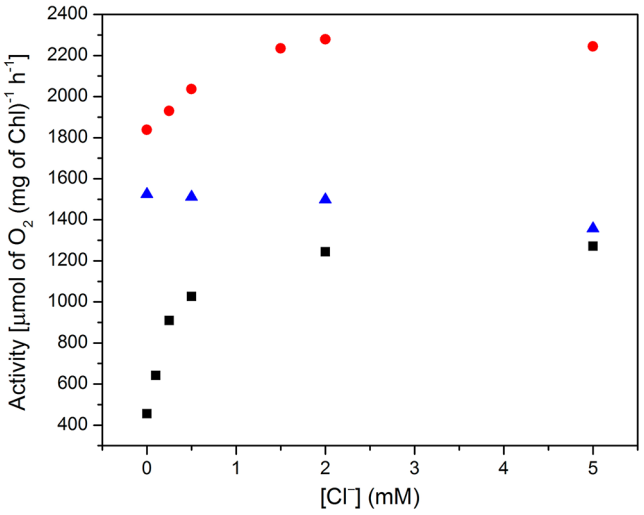

Figure 2. Oxygen-evolution activities of PSII core complexes isolated from the wild type (red circles), D2-K317A (blue triangles), and D2-K317R (black squares) as a function of added Cl^- concentration in the assay buffer. Oxygen-evolution rates were calculated using the first 30 s of data collected under illumination for each concentration of chloride. Oxygen-evolution traces showing oxygen evolution for a longer period (120 s under illumination) are shown in Figure S3 of the Supporting Information.

However, the D2-K317A PSII core complexes are still active for oxygen evolution. Therefore, Cl^- is required for turnover of the OEC only when a positively charged residue is present at the D2-K317 position. This supports our hypothesis that Cl^- is required for activity to prevent the formation of a salt bridge between the D2-K317 residue and the essential D1-D61 residue.

Fourier Transform Infrared Spectroscopy. The FTIR difference spectra induced by four successive flashes given to D2-K317R and D2-K317A PSII core complexes are compared to those of wild-type PSII in Figures 3 and 4, respectively. The corresponding spectra of D2-K317E and D2-K317Q PSII core complexes are shown in Figures S4 and S5 of the Supporting Information. The spectra that are induced by the first flash should correspond predominantly to S_2-minus-S_1 FTIR difference spectra.[58−61] The larger bands at 1706(−) and 1699(+) cm^{-1} in the first-flash FTIR difference spectra of D2-K317R, D2-K317Q, and D2-K317E probably reflect the flash-induced formation of $Y_Z^\bullet$ in the fractions of mutant PSII reaction centers that lack Mn_4Ca clusters. However, the features of the $Y_Z^\bullet$-minus-Y_Z FTIR difference spectrum are relatively small except for the 1706(−) and 1699(+) cm^{-1} bands and positive bands at 1550 and 1512 cm^{-1}.[44,62,63] Therefore, we conclude that the first-flash spectrum of all four mutants is dominated by the contributions of S_2-minus-S_1 spectra and not by contaminating features of $Y_Z^\bullet$-minus-Y_Z spectra.

To isolate the vibrational modes in the S_2-minus-S_1 FTIR difference spectrum that were altered by the D2-K317R and D1-K317A mutations and to display these alterations more clearly, the wild-type-minus-K317R and wild-type-minus-K317A double difference spectra were calculated (Figure 5, panels A and B, respectively). The NH_3^+ group of Lys gives rise to weak vibrational modes near 1626 and 1526 cm^{-1}.[64] Although it is possible that the 1629(+) and 1529(+) cm^{-1} bands in the wild-type-minus-K317R double difference spectrum and the 1627(+) and 1534(+) cm^{-1} bands in the

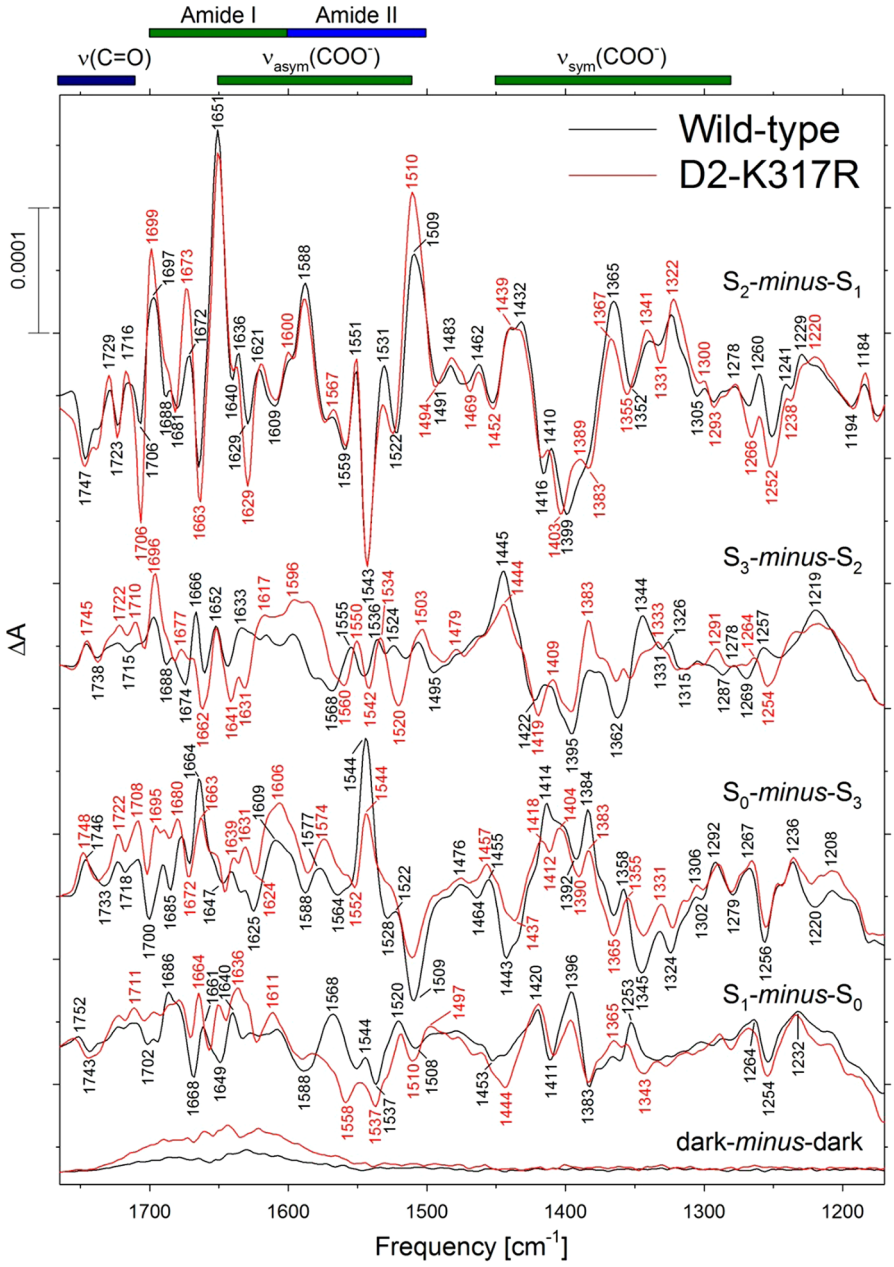

Figure 3. Comparison of the midfrequency FTIR difference spectra of wild-type (black) and D2-K317R (red) PSII core complexes in response to four successive flash illuminations applied at 0 °C. The wild-type PSII spectra correspond predominantly to the S_2-minus-S_1, S_3-minus-S_2, S_0-minus-S_3, and S_1-minus-S_0 FTIR difference spectra. The data (plotted from 1770 to 1170 cm^{-1}) represent the averages of 12 wild-type and 12 D2-K317R samples (14700 and 15800 scans, respectively). To facilitate comparisons, the D2-K317R spectra have been multiplied by a factor of 1.3 after normalization to the peak-to-peak amplitudes of the negative ferricyanide peak at 2115 cm^{-1} and the positive ferricyanide peak at 2038 cm^{-1}. Dark-minus-dark control traces are included to show the noise level (bottom traces).

wild-type-minus-K317A double difference spectrum reflect the loss of Lys NH_3^+ modes in the mutants, the bands may also arise from mutation-induced perturbations to amide or asymmetric carboxylate stretching [$\nu_{asym}(COO^-)$] modes. Similarly, the guanidyl group of Arg gives rise to relatively strong bands near 1672 and 1633 cm^{-1}.[64] Although a 1674(−) cm^{-1} band is present in the wild-type-minus-K317R double difference spectrum (Figure 5A), a similar band is present in the wild-type-minus-K317A double difference spectrum (Figure 5B), suggesting that this feature arises from mutation-induced alterations to amide vibrational modes. Both double difference spectra contain numerous additional features in their amide I and amide II/$\nu_{asym}(COO^-)$ regions, implying that both mutations alter the response of the polypeptide backbone to the $S_1 \rightarrow S_2$ transition. The double difference spectra also contain numerous features in their symmetric carboxylate stretching [$\nu_{sym}(COO^-)$] regions, specifically implying that both mutations perturb multiple carboxylate residues.

The D2-K317R PSII core complexes exhibited well-resolved second-, third-, and fourth-flash spectra that approximately resembled the S_3-minus-S_2, S_0-minus-S_3, and S_1-minus-S_0 FTIR difference spectra of the wild type, respectively (Figure 3). However, the amplitudes of these spectra were smaller than those of the corresponding spectra of wild-type PSII, especially

dx.doi.org/10.1021/bi301700u | Biochemistry 2013, 52, 4758−4773

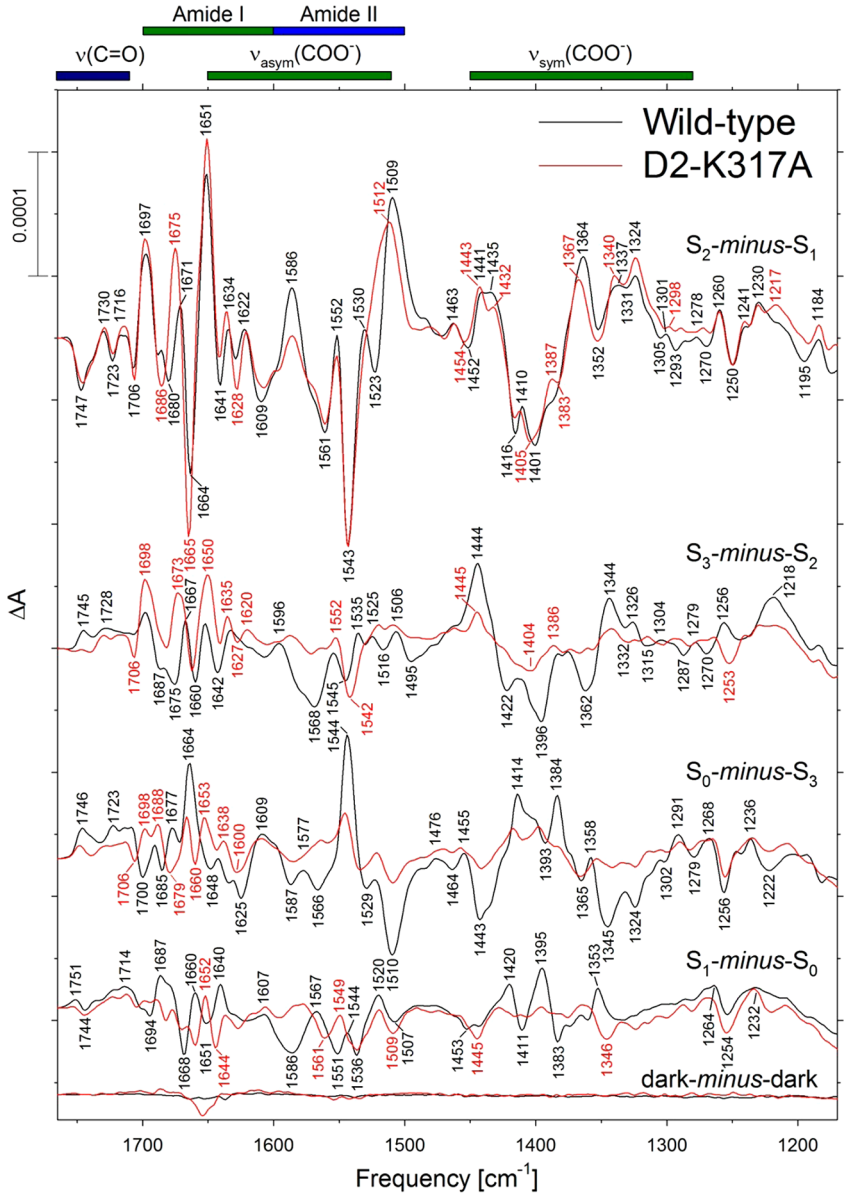

Figure 4. Comparison of the midfrequency FTIR difference spectra of wild-type (black) and D2-K317A (red) PSII core complexes in response to four successive flash illuminations applied at 0 °C. The wild-type spectra correspond predominantly to the S_2-minus-S_1, S_3-minus-S_2, S_0-minus-S_3, and S_1-minus-S_0 FTIR difference spectra. The data (plotted from 1770 to 1170 cm^{-1}) represent the averages of 14 wild-type and 14 D2-K317A samples (21600 and 21400 scans, respectively). To facilitate comparisons, the D2-K317A spectra have been multiplied by a factor of 1.04 after normalization to the peak-to-peak amplitudes of the negative ferricyanide peak at 2115 cm^{-1} and the positive ferricyanide peak at 2038 cm^{-1}. Dark-minus-dark control traces are included to show the noise level (bottom traces).

for the S_0-minus-S_3 difference spectrum, implying that the D2-K317R mutation increased the miss factor for S-state advancement. Notable differences from wild-type PSII that appear to be independent of the increased miss factor included bands at 1520(−) and 1383(+) cm^{-1} in the S_3-minus-S_2 difference spectrum, at 1639(+) and 1631(+) cm^{-1} in the S_0-minus-S_3 difference spectrum, and at 1558(−) and 1343(−) cm^{-1} in the S_1-minus-S_0 difference spectrum. These differences also imply that the D2-K317R mutation has slightly perturbed both carboxylate groups and polypeptide backbone conformations.

In striking contrast to D2-K317R, the D2-K317A, D2-K317Q, and D2-K317E mutations eliminated the 1523(−) cm^{-1} feature from the wild-type S_2-minus-S_1 difference spectrum (e.g., compare the two top traces in Figure 4). This feature was previously shown to be eliminated from the S_2-minus-S_1 FTIR difference spectrum of spinach PSII membranes after the depletion of Cl^- ions.[17] The D2-K317A, D2-K317Q, and D2-K317E mutations also decreased the amplitudes of the second-, third-, and fourth-flash difference spectra, respectively, to the point that they were almost featureless (Figure 4 and Figures S4 and S5 of the Supporting Information). Decreasing the interval between flashes from 13 to 3−4 s produced no increase in the amplitudes of these spectra. Some of the features in the second-flash spectra of these mutants [e.g., features at 1542(−), 1404(−), and 1253(−) cm^{-1}] resembled those in the S_2-minus-S_1 difference spectra. The elimination of the 1523(−) cm^{-1} mode by the D2-K317A mutation was manifested as a large negative feature at 1521 cm^{-1} in the wild-type-minus-K317A double difference spectrum (Figure 5B, black trace). To

dx.doi.org/10.1021/bi301700u | Biochemistry 2013, 52, 4758−4773

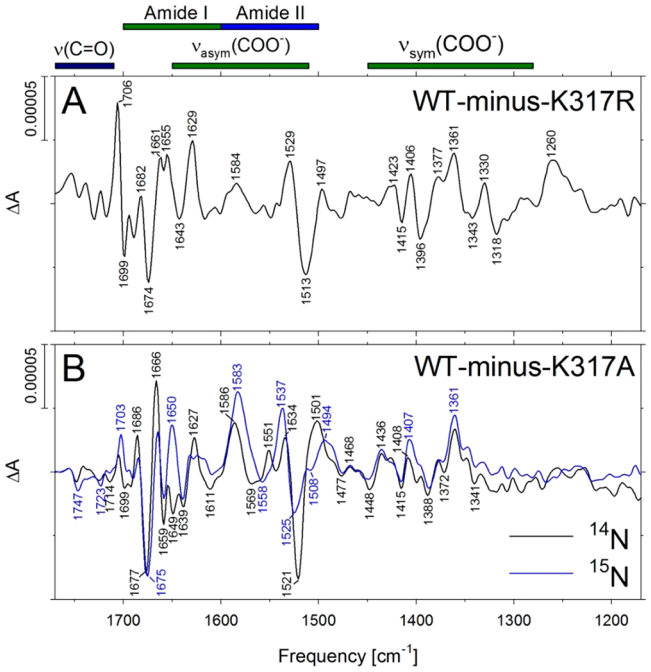

Figure 5. Double difference spectra (wild-type-minus-mutant) that were obtained by subtracting the S_2-minus-S_1 FTIR difference spectrum of D2-K317R (A) or D2-K317A (B) PSII core complexes from the S_2-minus-S_1 FTIR difference spectrum of wild-type PSII complexes. The spectrum obtained by subtracting the spectra of ^{15}N-labeled samples is shown as a blue line. The unlabeled double difference spectra in panels A and B were obtained by directly subtracting the S_2-minus-S_1 spectra in Figures 3 and 4, respectively. The ^{15}N-labeled double difference spectrum in panel B was obtained by subtracting the ^{15}N-labeled spectra shown in Figure S6 of the Supporting Information.

determine if this and other features between 1600 and 1500 cm^{-1} in the double difference spectrum correspond to changes in backbone amide II or $\nu_{asym}(COO^-)$ modes, both wild-type and D2-K317A PSII core particles were uniformly labeled with ^{15}N. A comparison of the midfrequency S_2-minus-S_1 FTIR difference spectra of unlabeled and ^{15}N-labeled wild-type and D2-K317A PSII core complexes is shown in Figure S6 of the Supporting Information. The S_2-minus-S_1 difference spectrum of ^{15}N-labeled wild-type PSII core complexes (Figure S6A of the Supporting Information, blue trace) closely resembles spectra reported previously for ^{15}N-labeled PSII preparations from spinach,[65] *Thermosynechococcus elongatus*,[66] and *Synechocystis* sp. PCC 6803.[45,46,67] In particular, the bands at 1552(+), 1543(−), 1530(+), and 1523(−) cm^{-1} have previously been identified as amide II modes because all four bands downshift 14−17 cm^{-1} after the global incorporation of ^{15}N[45,46,66,67] and 12−20 cm^{-1} after the global incorporation of ^{13}C.[45,66−68] The large positive band at 1586 cm^{-1} was previously assigned to a $\nu_{asym}(COO^-)$ mode because it is largely insensitive to the global incorporation of ^{15}N[45,66,67] but downshifts by 30−35 cm^{-1} after the global incorporation of ^{13}C.[45,66−68] The S_2-minus-S_1 difference spectrum of ^{15}N-labeled D2-K317A PSII core complexes (Figure S6B of the Supporting Information, blue trace) showed similar ^{15}N-induced shifts. In particular, the global incorporation of ^{15}N shifted the positive feature from 1552 to 1537 cm^{-1} and the negative feature from 1543 to 1529 cm^{-1}.

The wild-type-minus-K317A double difference spectrum of ^{15}N-labeled samples is compared to that of the unlabeled samples in Figure 5B. The global incorporation of ^{15}N substantially decreased the amplitudes of the 1521(−) and 1501(+) cm^{-1} features in the wild-type-minus-K317A double difference spectrum (Figure 5B, blue traces). To explain these changes, we propose that the 1523(−) cm^{-1} feature in the wild-type S_2-minus-S_1 FTIR difference spectrum (Figure 4, top black trace, or Figure S6A of the Supporting Information, black trace) corresponds to an amide II mode that is downshifted underneath the 1509(+) cm^{-1} feature by the global incorporation of ^{15}N, thereby decreasing the amplitude of the latter. Incorporation of ^{15}N would cause a smaller decrease in the magnitude of the corresponding 1512(+) cm^{-1} feature in the D2-K317A S_2-minus-S_1 FTIR difference spectrum (Figure S6B of the Supporting Information) because there is no 1523(−) cm^{-1} mode to shift beneath the 1512(+) cm^{-1} feature in this spectrum. We conclude that the elimination of the 1523(−) cm^{-1} mode by the D2-K317A mutation reflects a substantial change in the response of the polypeptide backbone to the positive charge that develops on the Mn_4Ca cluster during the $S_1 \rightarrow S_2$ transition. Because the same mode is eliminated by the D2-K317E and D2-K317Q mutations (Figures S4 and S5 of the Supporting Information), but not by the D2-K317R mutation, we conclude that the D2-K317A, D2-K317Q, and D2-K317E PSII mutations perturb the structure of PSII substantially more than the D2-K317R mutation. These perturbations likely prevent normal S-state cycling in the D2-K317A, D2-K317Q, and D2-K317E mutants under the conditions of the FTIR measurements. The FTIR data were obtained in response to single actinic flashes spaced 13 s apart. Consequently, the near elimination of spectral features after the second, third, and fourth flashes in D2-K317A, D2-K317Q, and D2-K317E PSII core complexes indicates that either the efficiency of S-state advancement beyond the S_2 state is sharply decreased or the stability of the S_3 state is sharply diminished by the D2-K317A, D2-K317E, and D2-K317Q mutations.

Electron Paramagnetic Spectroscopy. EPR spectra of wild-type, D2-K317R, and D2-K317A PSII were obtained in the S_1 and S_2 states (Figure 6). The cytochrome c_{550} signal was observed in the dark in wild-type, D2-K317R, and D2-K317A PSII. Once the centers had reached the S_2 state, a $g = 2$ multiline signal was observed in wild-type, D2-K317R, and D2-K317A PSII. The $g = 2$ multiline signals in D2-K317R and D2-K317A PSII had peak positions similar to those of the $g = 2$ multiline signal in the wild type. Interestingly, a $g = 4$ signal was observed in D2-K317R in addition to the $g = 2$ multiline signal (Figure 6). The $g = 4$ signal was not observed in wild-type or D2-K317A PSII. In addition to the S_2-state signals from the OEC, an oxidized cytochrome b_{559} $g = 3$ signal was also generated by 200 K illumination of wild-type, D2-K317R, and D2-K317A PSII. The oxidized cytochrome b_{559} signal originated from the fraction of centers lacking the OEC. On the basis of the total chlorophyll content of the wild-type, D2-K317R, and D2-K317A EPR samples, the S_2-state EPR signal intensities were much weaker for D2-K317A and D2-K317R on a per chlorophyll basis. This indicates that the fraction of PSII cores with an intact OEC in the D2-K317R and D2-K317A cores is much lower than the fraction of PSII cores with an intact OEC in the wild-type sample. Lower yields of the assembled OEC in D2-K317A and D2-K317R PSII cores can

dx.doi.org/10.1021/bi301700u | *Biochemistry* 2013, 52, 4758−4773

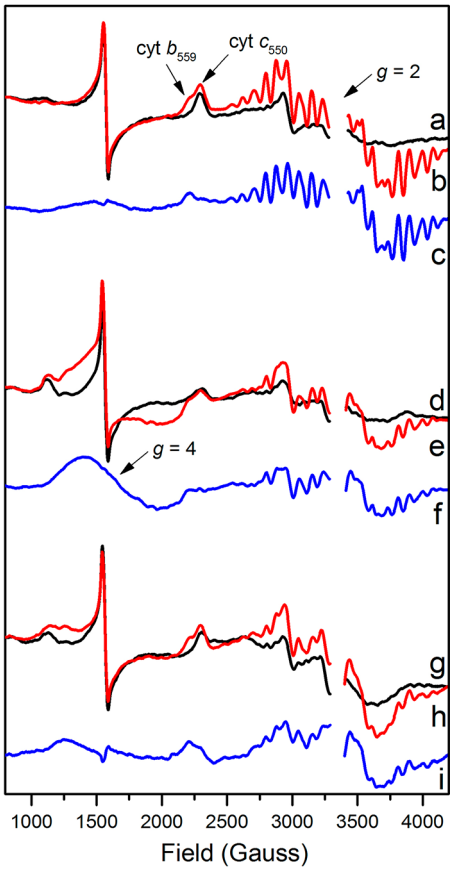

Figure 6. S_1-state (black), S_2-state (after 200 K illumination, red), and S_2-minus-S_1 (blue) difference spectra of wild-type, D2-K317R, and D2-K317A PSII. Wild-type S_1-state spectrum (a), wild-type S_2-state spectrum (b), wild-type S_2-minus-S_1 difference spectrum (c), D2-K317R S_1-state spectrum (d), D2-K317R S_2-state spectrum (e), D2-K317R S_2-minus-S_1 difference spectrum (f), D2-K317A S_1-state spectrum (g), D2-K317A S_2-state spectrum (h), and D2-K317A S_2-minus-S_1-state spectrum (i). The g = 4 signal in the D2-K317R S_2-minus-S_1 difference spectrum, the g_z signals of cytochrome b_{559} and cytochrome c_{550} in the WT S_1- and S_2-state spectra, and the g = 2 multiline signal in the WT S_2-state spectra are labeled.

also explain the low oxygen-evolution activity of the D2-K317A and D2-K317R PSII cores.

O_2 Flash Yields and Kinetics of O_2 Release. Flash-induced oxygen yield measurements of D2-K317A and D2-K317R PSII core complexes at 22 °C showed a period four oscillation pattern. However, the oscillatory patterns for D2-K317A and D2-K317R PSII were more dampened than the pattern for wild-type PSII, as shown in Figure 7. When the O_2 yields were fit with a four-state model including misses and double hits parameters, higher miss factors were observed for D2-K317A and D2-K317R PSII in the following order: D2-K317A > D2-K317R > wild type (Table 1). In our fitting procedure for the data obtained for wild type and D2-K317R PSII, all parameters were set to be free, whereas the double hits parameter and the S_0-state population had to be constrained for D2-K317A to obtain reasonable output.

As noted earlier, our FTIR data indicate that either the efficiency of S-state advancement beyond the S_2 state is sharply decreased or the stability of the S_3 state is sharply diminished by the D2-K317A, D2-K317E, and D2-K317Q mutations. The FTIR data were obtained at 0 °C with 13 s flash spacing.

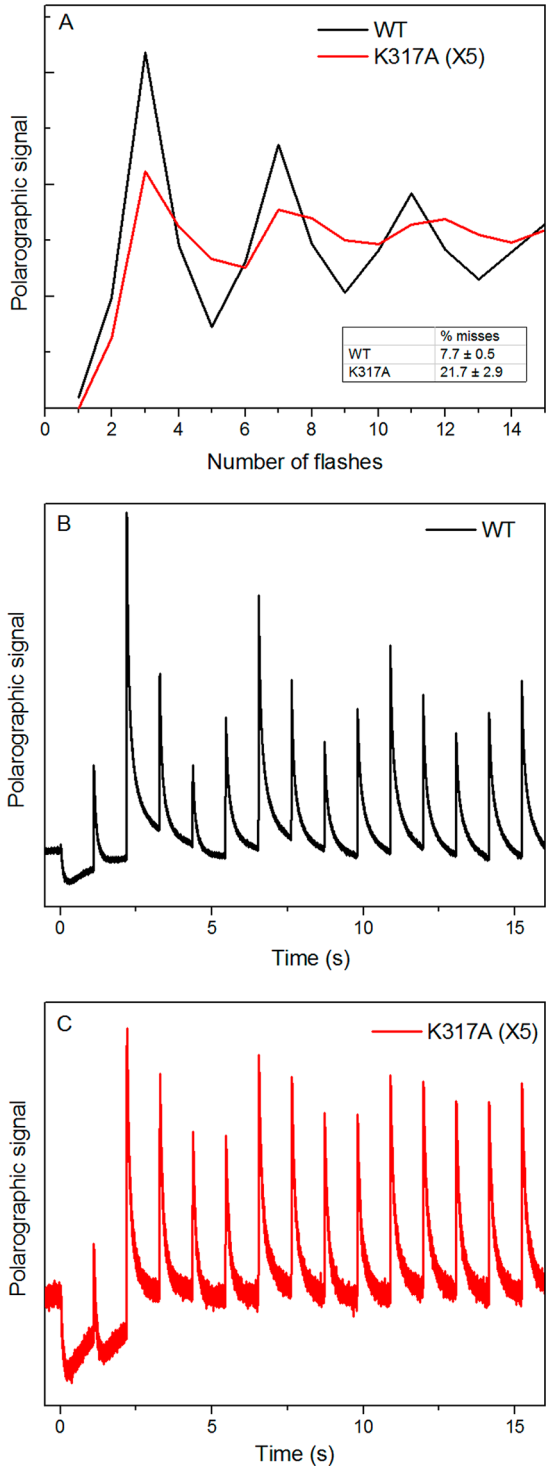

Figure 7. (A) Comparison of the flash O_2 yield patterns of wild-type (black) and D2-K317A (red) PSII at 22 °C in response to 15 saturating flashes from a xenon lamp applied at a frequency of 1 Hz. The percent misses, calculated according to the fit created using a four-state model, are shown as an inset for both wild-type and D2-K317A PSII. (B and C) Amperometric signal obtained in response to 1 Hz flashes for wild-type PSII cores (panel B, black), and D2-K317A PSII cores (panel C, red). The signal intensity for wild-type PSII is roughly 5-fold higher than that for D2-K317A PSII.

However, all three mutants were photoautotrophic, and steady-state O_2-evolution measurements showed that all three mutants advance through the S states at 25 °C. To further investigate

dx.doi.org/10.1021/bi301700u | *Biochemistry* 2013, 52, 4758−4773

Table 1. Comparison of Misses, Double Hits, and S-State Populations of Wild-Type (WT) and D2-K317A PSII Cores Obtained from the Fits of the Flash O_2 Yield Patterns[a]

	misses, α (%)	double hits, β (%)	S_0 (%)	S_1 (%)	S_2 (%)	S_3 (%)
WT	7.7 ± 0.5	7.0 ± 0.3	19.0 ± 1.5	71.1 ± 1.8	9.6 ± 1.7	1.7 ± 0.6
D2-K317R	17.6 ± 0.1	5.2 ± 0.1	20.0 ± 0.3	68.5 ± 0.5	7.7 ± 0.2	3.8 ± 0.0
D2-K317A	21.7 ± 2.9	7.6*	20.0*	69.1 ± 2.0	8.6 ± 1.9	2.3 ± 0.2

[a]For wild-type and D2-K317R PSII, the constraints were as follows: 0% ≤ α ≤ 50%, 0% ≤ β ≤ 33%, and 0% ≤ S_0, S_1, S_2, S_3. For D2-K317A PSII, the constraints were as follows: 0% ≤ α ≤ 50% and 0% ≤ S_1, S_2, S_3. Double hits (β) and the S_0-state population for D2-K317A (noted with asterisks) were constrained to be similar to those in the wild-type data.

the apparent discrepancy between these observations, we conducted flash-based polarographic measurements at 0 °C using different flash spacings for D2-K317A PSII. Amperometric signals were observed for flash spacings of 500 ms, 1.1 s, 3.3 s, and 14.3 s, implying that the $S_2 \rightarrow S_3$ transition takes place at 0 °C (Figure S8 of the Supporting Information). At 500 ms and 1.1 s flash intervals, maximal currents appeared at the third and seventh flashes in D2-K317A PSII. This is similar to what is observed for wild-type PSII (Figure S7 of the Supporting Information). However, the oscillatory pattern is significantly dampened in the case of D2-K317A PSII. These results agree with results obtained at 22 °C. The high miss factor for D2-K317A PSII cores explains the increased dampening.

However, at 3.3 and 14.3 s flash intervals, the oscillatory pattern of amperometric signals from D2-K317A PSII is quite different from what is observed at 500 ms and 1.1 s flash intervals. The oscillatory patterns at longer flash intervals do not follow the classic period four pattern and are significantly more dampened (Figures S7 and S8 of the Supporting Information). The dampening of the oscillatory pattern is related to an increase in percent misses. From these results, we propose that the $S_2 \rightarrow S_3$ transition takes place at 0 °C but that the S_3 state is much more short-lived in D2-K317A PSII than it is in wild-type PSII. Because the flash interval for the FTIR measurements was 13 s, we believe that once the OEC was advanced to the S_3 state, the S_3 state decayed back to the S_2 state on a relatively short time scale, thereby essentially giving an S_2-minus-S_2 spectrum in a majority of D2-K317A PSII reactions centers over the data averaging time of 13 s.

The O_2-release kinetics of wild-type, D2-K317A, and D2-K317R PSII were investigated at 22 °C (Figure 8). Additionally, O_2-release kinetics of wild-type and D2-K317A were also measured at 0 °C (Figure S9 of the Supporting Information). D2-K317A and D2-K317R PSII have a slower rise time and a slower decay time when compared to those of wild-type PSII. The observed O_2-release kinetics decreased in the following order: wild type > D2-K317R > D2-K317A (Figure 8). The O_2-release kinetics are consistently slower for both wild-type and D2-K317A PSII at 0 °C (Figure S9 of the Supporting Information). Retardation in O_2 release has also been observed in the D1-D61 and CP43-R357 mutants.[71−74] Because CP43-R357, D1-D61, and D2-K317 are in the same hydrogen-bonding network, it is reasonable that disrupting this hydrogen-bonding network would have a similar effect on the kinetics of the $S_3 \rightarrow [S_4] \rightarrow S_0$ step. These mutations effectively decrease the efficiency of deprotonation events in the $S_3 \rightarrow [S_4] \rightarrow S_0$ step. Interestingly, a lag phase of a few milliseconds is observed before the rise of the amperometric signal in the polarographic data for D2-K317A PSII cores at 0 °C (Figure S9 of the Supporting Information). This is similar to what has been observed in the D1-D61N mutant.[71] Hence, we can conclude that the deprotonation events important for the $S_3 \rightarrow [S_4] \rightarrow S_0$ transition are less efficient in the D2-K317A and D2-K317R mutants.

DISCUSSION

Our results indicate that the steady-state oxygen-evolution activity of D2-K317A PSII is independent of Cl^-. This result is consistent with our hypothesis that the D2-K317A mutation results in the loss of Cl^- binding at the D2-K317 site. The D2-K317A mutation causes substantial changes to the amide and carboxylate vibrational modes in PSII, as observed by FTIR. Some of these changes resemble those observed previously in Cl^--depleted PSII membranes from spinach.[17] Similar changes were observed in FTIR spectra of D2-K317Q and D2-K317E PSII. On the other hand, the D2-K317R mutation caused substantially fewer structural perturbations as observed by FTIR, and S-state cycling under the conditions of the FTIR experiments was almost normal in D2-K317R PSII, although with an apparently higher miss factor. The steady-state oxygen-evolution activity of D2-K317R PSII was dependent on Cl^- with an effective K_D for Cl^- binding higher than of the wild type. We have proposed that the Cl^- effect in wild-type PSII comes about due to the formation of a salt bridge between D1-D61 and D2-K317 upon removal of Cl^- from this site.[4,34] Our results support the hypothesis that chloride is required for activity only when a positively charged residue is present at the D2-K317 position. In the D2-K317A mutant, the D1-D61 residue cannot form a salt bridge with D2-A317 even in the absence of Cl^-. Therefore, D2-K317A is active even in the absence of chloride. However, the D1-D61 residue is capable of forming a salt bridge with D2-R317 in the absence of chloride, and thus, the chloride requirement is preserved in the D2-K317R mutant. Therefore, one role of chloride at the D2-K317 site is to shield an essential carboxylate (D1-D61) from forming a salt bridge with D2-K317. In the absence of chloride, D1-D61 forms a salt bridge with D2-K317, thereby limiting the transport of a proton from the OEC to the lumen. In addition to shielding D1-D61 from D2-K317, chloride at the D2-K317 site could also play a second role of fine-tuning the pK_a of D1-D61 and optimally position D1-D61 for efficient proton removal. Lower oxygen evolving activities of D2-K317A and D2-K317R are either due to a slower k_{cat} for water oxidation at the OEC, due to perturbations of the hydrogen-bonding network, or due to a smaller percentage of the assembled OEC in the mutants, or both. Disruption of the hydrogen-bonding network required for proton removal could result in a lower k_{cat} for D2-K317A and D2-K317R PSII.

Similar effects of mutations have been observed in other Cl^--activated enzymes such as α-amylase and angiotensin-converting enzyme (ACE). In α-amylase and ACE, the mutation of a positively charged residue in the Cl^--binding pocket to a neutral residue results in decreased enzyme activity

dx.doi.org/10.1021/bi301700u | Biochemistry 2013, 52, 4758−4773

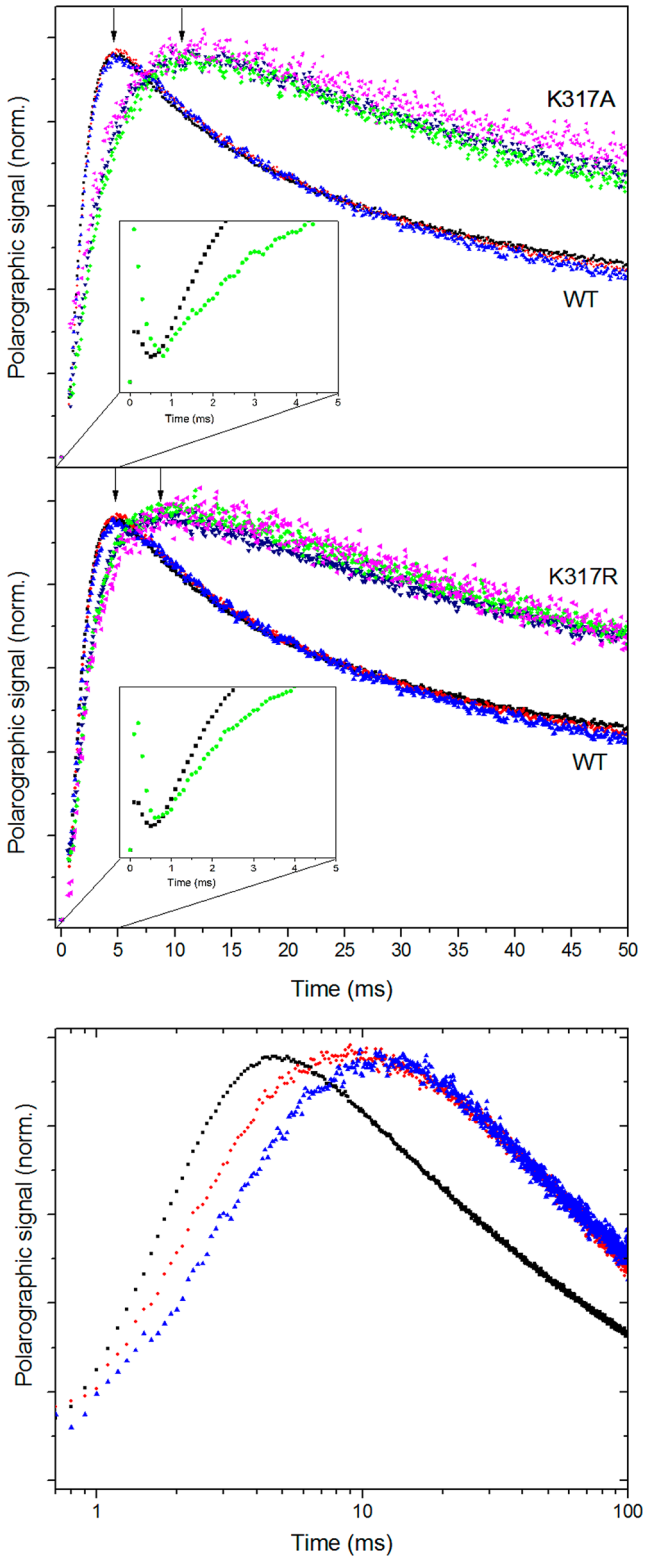

Figure 8. Oxygen-release kinetics of wild-type, D2-K317A, and D2-K317R PSII cores at 22 °C. The top panel shows a comparison between the wild type and D2-K317A, and the middle panel shows a comparison between the wild type and D2-K317R. Amperometric signals obtained for wild-type PSII cores on the third, fourth, and fifth flashes (black, red, and blue, respectively) are shown in both panels. Amperometric signals obtained for D2-K317A and D2-K317R PSII cores on the third, fourth, and fifth flashes (green, navy, and magenta, respectively) are shown in the top and middle panels, respectively. All the amperometric signals are normalized to the same peak current. Arrows indicate peak current positions. A flash artifact appearing within 500 μs to 1 ms of the flash has been omitted from all data. The insets show the initial 5 ms of the normalized third-flash signal of the wild-type (WT, black) and D2-K317A and -R (green) PSII cores without removal of the flash artifact. The bottom panel shows a comparison of amperometric signals of the wild type (black), D2-K317R (red), and D2-K317A (blue) plotted vs a logarithmic time scale.

that is independent of Cl^-.[75,76] Interestingly, the crystal structures of the active sites of the N298S mutant of α-amylase with and without Cl^- show some significant differences in the positioning of the amino acids, with the most important difference being the movement of a Glu residue toward the vacant Cl^- site to form a salt bridge with the R195 residue.[4,76−81] The loss of activity upon Cl^- removal in the N298S mutant can be directly correlated to these structural and electrostatic changes in the active site. These aforementioned results from α-amylase and ACE in conjunction with our results from D2-K317A PSII suggest that Cl^--independent activity can be achieved in PSII.

The S_2-state EPR spectrum of D2-K317A PSII shows that the OEC gives a g = 2 multiline signal with peak positions and line widths similar to those of the signal observed for the wild type (Figure 6). In spinach, removal of Cl^- and its substitution with some other monovalent anions and primary amines give rise to a broad g = 4.1 signal in place of the g = 2 multiline signal. We had proposed earlier that the origin of the g = 4.1 signal is associated with structural and electronic perturbations related to the formation of a salt bridge between D1-D61 and D2-K317 upon Cl^- removal.[4] Because the D2-K317A mutant has lost the ability to form a salt bridge between the D1-D61 and D2-A317 residues, the absence of the g = 4 signal in the D2-K317A mutant PSII cores is in agreement with our proposal. However, the g = 4 signal has been observed in only I^-- or Sr^{2+}-substituted cyanobacterial PSII, and not under Cl^--depleted conditions.[22] There is evidence from our work that the conditions that are optimal for the removal of Cl^- from spinach PSII are ineffective for the removal of Cl^- from PSII isolated from *Synechocystis*, suggesting that the K_D of Cl^- binding is different in PSII isolated from plants and cyanobacteria.

However, a g = 2 multiline signal and a broad g = 4 signal are observed in the S_2-state EPR spectrum of D2-K317R under chloride sufficient conditions (Figure 6). A similar g = 4 signal has been observed in I^--substituted cyanobacterial PSII. The mechanism of origin of the g = 4 signal in an I^--substituted PSII must be different from the mechanism of origin of the g = 4 signal in "chloride-depleted" PSII. When the chloride ion is substituted with a larger iodide ion, there is "crowding" in the chloride-binding site, which will lead to repositioning of the nearby residues, possibly creating a state that stabilizes the centers that give rise to the g = 4 signal. Substitution of the lysine residue at the D2-K317 position with a longer arginine residue will also lead to crowding in the chloride-binding site, thereby causing similar structural changes that may stabilize the centers that give rise to the g = 4 signal.

It is interesting that a g = 4 S_2-state EPR signal is observed in the D2-K317R PSII sample, but this signal has not been previously observed in "Cl^--depleted" wild-type cyanobacterial PSII. This may be due to tight binding of chloride in the wild-

dx.doi.org/10.1021/bi301700u | *Biochemistry* 2013, 52, 4758−4773

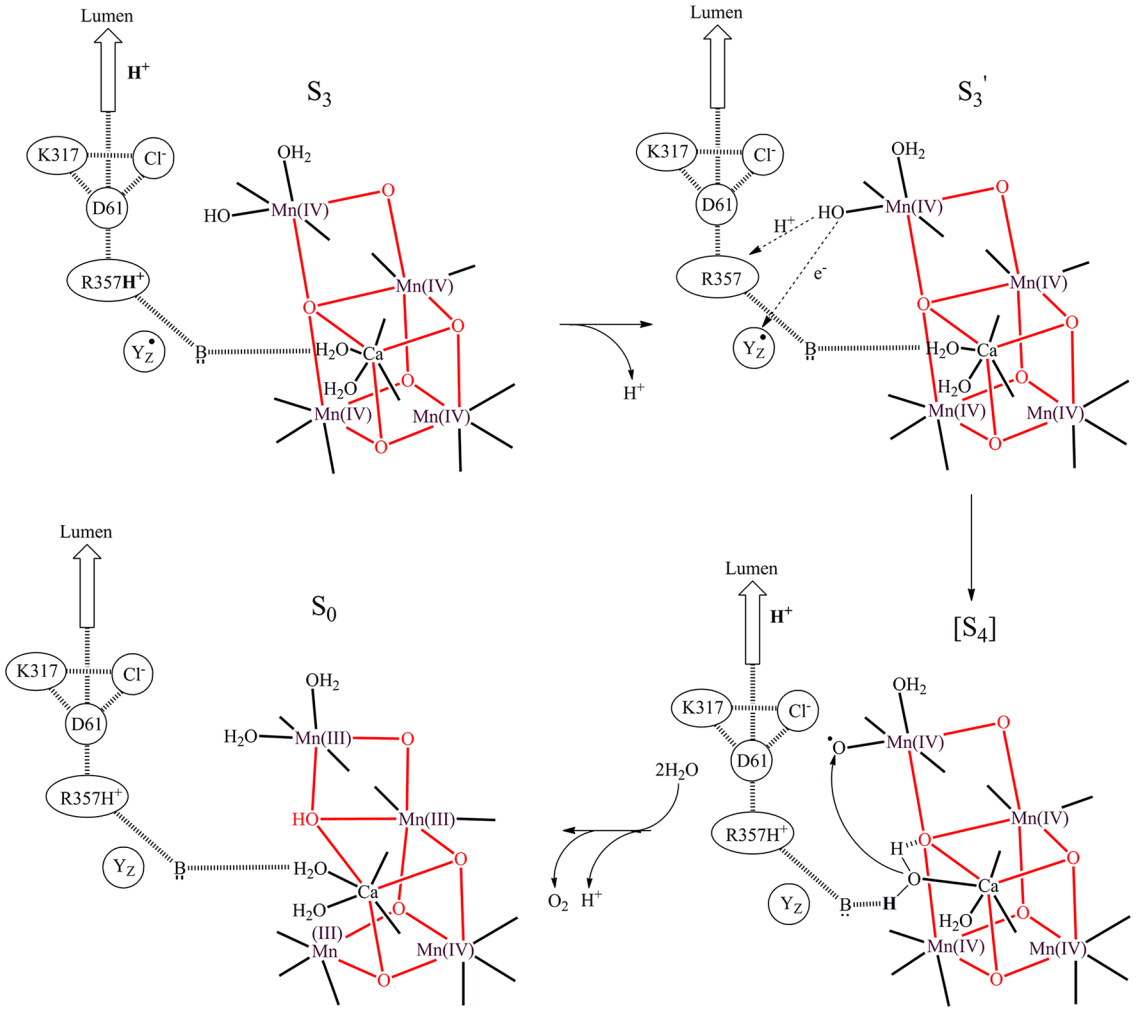

Figure 9. Proposed mechanism for the wild-type $S_3 \rightarrow [S_4] \rightarrow S_0$ transition. In the first step, an electrostatic interaction between the CP43-R357 residue and $Y_Z^{\bullet}$ results in deprotonation of the CP43-R357 residue. The proton leaves via a proton exit pathway gated by the triad of D1-D61, D2-K317, and Cl^-. Next, a proton-coupled electron transport occurs in which the proton from the Mn(IV)−OH moiety in the OEC moves to the CP43-R357 residue while $Y_Z^{\bullet}$ is oxidized to the OEC. A Mn(IV)−$O^{\bullet}$ moiety is produced as a result of the oxidation. Nucleophilic attack by the Ca-bound water on the Mn(IV)−$O^{\bullet}$ moiety in tandem with deprotonation of the Ca-bound water results in O−O bond formation. One of the protons protonates a bridging oxo, while the other proton moves to the lumen via the proton exit pathway. It has been postulated that the $S_3' \rightarrow [S_4]$ transition is the rate limiting step for O−O bond formation in wild-type PSII. However, in some mutants such as the D2-K317 and D1-D61 mutants, an inefficient proton-relay network might make the $[S_4] \rightarrow S_0$ transition rate-limiting for O−O bond formation and O_2 release. If so, it is theoretically feasible to trap the $[S_4]$ state in some of these mutant PSII samples.

type cyanobacterial PSII sample such that chloride remains bound even in a "Cl^--depleted" sample, consistent with our oxygen-evolution assays, whereas weaker chloride binding in spinach PSII results in a $g = 4$ S_2-state EPR signal in a "Cl^--depleted" spinach PSII sample. Thus, the different behavior between spinach and cyanobacterial PSII with regard to observation of a $g = 4$ S_2-state EPR signal may simply reflect tighter chloride binding in cyanobacterial PSII.

Flash-induced oxygen yield experiments suggest that D2-K317A and D2-K317R have a higher percentage of misses during the S-state transitions as compared to the misses in wild-type PSII cores (Figure 7 and Table 1). This leads to a dampened oscillatory pattern for D2-K317A and D2-K317R PSII. The increase in misses could be related to the inefficient transport of a proton from the OEC to the lumen. The D2-K317 residue is 11.9 Å from Y_Z and 6.7 Å from the OEC. Hence, the mutation of this residue should have little effect on the reduction potentials of Y_Z and the OEC, especially considering a net zero change in charge when the D2-$K317^+$/Cl^- pair is substituted with a neutral A residue alone. Similarly, a conservative D2-K317R mutation should have an even weaker effect on the reduction potentials of Y_Z and the OEC. However, the D2-K317A mutation (as well as the absence of chloride) and the D2-K317R mutation will have a pronounced effect on the hydrogen-bonding network that is important for proton exit (see Figure 1). Recently, there has been increased interest in studying the role of the hydrogen-bonding network for efficient water oxidation catalysis in PSII.[62,82,83] It has been shown that the hydrogen-bonding network including D1-D61, D1-E65, and D2-E312 spans large distances within the protein.[62] The robustness of the hydrogen-bonding network will correlate with the efficiency of proton-transfer steps, which will have a pronounced effect on transitions involving proton release. Other than disrupting the hydrogen-bonding network, the D2-K317A mutation (and the absence of Cl^-) and the D2-K317R mutation could also have an effect on the pK_a values and positions of the nearby charged residues, such as the D1-D61 residue, involved in the proton-transfer network.

dx.doi.org/10.1021/bi301700u | *Biochemistry* 2013, 52, 4758−4773

The FTIR results imply that the D2-K317A, D2-K317Q, and D2-K317E PSII do not efficiently cycle through all the S states when a 13 s flash spacing is used at 0 °C (Figure 4 and Figures S4 and S5 of the Supporting Information). The characteristic period four oscillation patterns in the polarographic measurements of D2-K317A PSII confirm that D2-K317A PSII cycles through all of the S states at 0 °C. Hence, we believe that a faster decay of the S_3 state of the OEC in D2-K317A PSII (and in D2-K317Q and D2-K317E) leads to the inability to obtain the S_3-minus-S_2 and S_0-minus-S_3 FTIR difference spectra when a 13 s flash spacing is used at 0 °C. This apparent destabilization of the S_3 state in the D2-K317A, -Q, and -E mutants may also be related to the ineffective transport of a proton from the OEC to the lumen. A higher percentage of misses and a less stable S_3 state of the OEC could also affect the efficiency of the assembly process of the OEC in D2-K317A mutant cells. As discussed above, a smaller fraction of the assembled OEC in the D2-K317A cores, also confirmed by the EPR results, can explain the loss in total activity of this mutant.

The O_2-release kinetics is of great interest because we can obtain information about the kinetics of the $S_3 \rightarrow [S_4] \rightarrow S_0$ transition. The O_2-release kinetics is directly correlated with the removal of a proton from the OEC in this transition. A time-resolved XAS study suggested that a deprotonation event precedes a proton-coupled electron transfer from the OEC to $Y_Z^{\bullet}$ in the $S_3 \rightarrow [S_4] \rightarrow S_0$ transition.[69] A lag phase between the time of the flash and the rise of an amperometric signal is caused by this early deprotonation event. Furthermore, time-resolved XAS and time-resolved absorption spectroscopy indicate that the rate-determining step for O−O bond formation is the transfer of an electron from the OEC to $Y_Z^{\bullet}$.[69,70] However, this electron transfer is coupled to a proton transfer before O_2 release. Therefore, slowing the kinetics of proton release can also slow the O_2-release kinetics.

As shown in Figure 8 and Figure S9 of the Supporting Information, the O_2-release kinetics of D2-K317A PSII is slower than that of wild-type PSII at both 22 and 0 °C. The O_2-release kinetics of D2-K317R is also slower than that of the wild type, but slightly faster than that of D2-K317A (Figure 8). The O_2-release kinetics is a direct probe of the $S_3 \rightarrow [S_4] \rightarrow S_0$ transition. The slower release kinetics unequivocally indicates that the $S_3 \rightarrow [S_4] \rightarrow S_0$ transition is slower in D2-K317A and D2-K317R PSII. This transition is not well characterized and has not been studied in much detail. However, there have been some important experiments that suggest a sequence of proton-transfer and electron-transfer events take place in this transition. It is known that this transition results in a net release of two protons from PSII to the lumen. Time-resolved XAS and time-resolved UV−visible experiments have shown that a deprotonation event takes place when Y_Z is oxidized to $Y_Z^{\bullet}$, and before the OEC advances past the S_3 state.[69,70] The CP43-R357 residue is a strong candidate proposed for being deprotonated as a result of an electrostatic interaction with $Y_Z^{\bullet}$ during this step (Figure 9).[28] Immediately following the deprotonation event, a proton-coupled electron transfer is proposed to take place in which the electron is transferred from the OEC to $Y_Z^{\bullet}$ and the proton is transferred from the Mn(IV)−OH moiety to a basic residue, possibly CP43-R357. This PCET will advance the OEC from the S_3 state to the $[S_4]$ state, where a Mn(IV)-$O^{\bullet}$ moiety is ready for nucleophilic attack from a Ca-bound water molecule (Figure 9). The nucleophilic attack will result in O−O bond formation, which is followed or accompanied by the removal of two protons from the Ca-bound water, one of which is proposed to protonate the O5 oxo bridge of the OEC and the other of which is proposed to move through the proton exit pathway to the lumen (Figure 9). Hence, the $S_3 \rightarrow [S_4] \rightarrow S_0$ transition has a net loss of two protons.

By analyzing the positioning of the residues that could be involved in the exit of a proton from the OEC, we propose that the same proton-relay network is active when each of the two protons is transported, albeit at different times, from the OEC to the lumen in the $S_3 \rightarrow [S_4] \rightarrow S_0$ transition. The four water molecules on the OEC are strongly hydrogen bonded and share, via some water molecules, the same hydrogen-bonding network with the CP43-R357 residue, the D1-D61 residue, the D2-K317 residue, and Cl^-. We propose that a triad comprised of D1-D61, D2-K317, and Cl^- (Figures 1 and 9) functions in gating protons from the OEC to the lumen. The CP43-R357 residue shares the hydrogen-bonding network with the triad. Therefore, any significant change in the triad or in the CP43-R357 residue will result in slower kinetics of oxygen release during the $S_3 \rightarrow [S_4] \rightarrow S_0$ transition. Similarly, the lag phase observed between the flash and the rise of the amperometric signal, resulting from a deprotonation event, is also expected to be longer when significant changes are made to the proton-relay network involving the CP43-R357 residue and the triad. Slower O_2-release kinetics have been observed for the D1-D61N, D1-D61A, and CP43-R357K mutants.[71−74] Surprisingly, the D1-D61E mutant has O_2-release kinetics similar to that of the wild type,[73] possibly because of the more conservative mutation having little effect on the hydrogen-bonding network and removal of a proton from the OEC. However, the D2-K317R mutant has a slightly slower O_2-release kinetics. Interestingly, the CP43-E354Q mutation, which is a mutation of one of the ligands to the OEC, does not change the O_2-release kinetics. The CP43-E354Q mutation does cause lower steady-state oxygen-evolution rates (20% of that of wild-type PSII), accelerated substrate water exchange rates, an altered structure of the OEC, and a longer lifetime of the S_2 state of the OEC. The CP43-E354 residue does not partake in the proton removal network and, therefore, has little effect on the oxygen-release kinetics in the $S_3 \rightarrow [S_4] \rightarrow S_0$ transition. The results obtained from our work and from previous work on other mutants strongly suggest that disruption of the proton-removal pathway slows oxygen release in the $S_3 \rightarrow [S_4] \rightarrow S_0$ transition. Although it has been suggested that the rate-limiting step in O−O bond formation in wild-type PSII is the transfer of an electron from the OEC to $Y_Z^{\bullet}$, we believe that the rate-limiting step can be changed to proton transfer in some of these mutations and under harsh pH conditions. A similar change in the rate-limiting step of a PCET process has been observed in bacterial reaction centers, where a number of mutations change the rate-limiting step in $Q_B^{\bullet -}$ reduction from electron transfer to proton transfer.[84] Hence, in situations where the hydrogen-bonding network around the OEC in PSII is disrupted by mutations in D2-K317, D1-D61, and CP43-R357, we propose that the rate-limiting step for O−O bond formation is proton transfer in the $S_3 \rightarrow [S_4] \rightarrow S_0$ transition. Therefore, under these conditions, it is possible that a longer-lived $[S_4]$ intermediate can persist. Further work needs to be done to attempt to trap the $[S_4]$ intermediate using the D1-D61, CP43-R357, and D2-K317 mutants that lead to slower oxygen-release kinetics.

dx.doi.org/10.1021/bi301700u | Biochemistry 2013, 52, 4758−4773

■ ASSOCIATED CONTENT

Supporting Information

Growth curves in normal media and "chloride-free media", SDS−polyacrylamide gel showing the presence of extrinsic subunits in the D2-K317 mutants, FTIR spectra of D2-K317E and D2-K317Q PSII core complexes, FTIR of globally ^{15}N-labeled wild-type and D2-K317A PSII core complexes, flash oxygen yields at 0 °C with varied flash spacing, and kinetics of flash-induced oxygen release at 0 °C. This material is available free of charge via the Internet at http://pubs.acs.org.

■ AUTHOR INFORMATION

Corresponding Author

*G.W.B.: e-mail, gary.brudvig@yale.edu; phone, (203) 432-5202; fax, (203) 432-6144. R.J.D.: e-mail, richard.debus@ucr.edu; phone, (951) 827-3483; fax, (951) 827-4294.

Present Address

[§]R.J.S.: Zilkha Neurogenetic Institute, University of Southern California, Los Angeles, CA 90093.

Funding

This work was supported by grants from the Department of Energy, Office of Basic Energy Sciences, Division of Chemical Sciences. Oxygen-release and EPR studies were supported by Grant DE-FG02-05ER15646 (to G.W.B.). Mutant Construction and FTIR studies were supported by Grant DE-FG02-10ER16191 (to R.J.D.).

Notes

The authors declare no competing financial interest.

■ ACKNOWLEDGMENTS

We are grateful to Anh P. Nguyen for constructing the mutants, purifying the thylakoid membranes that were used to purify PSII for the FTIR experiments, and conducting the SDS−PAGE analysis, Norton Kitagawa for performing the MALDI mass spectrometry measurements of the SDS−PAGE bands, and Takumi Noguchi and Peter Nixon for communicating results prior to publication.

■ ABBREVIATIONS

ACE, angiotensin-converting enzyme; Chl, chlorophyll; CP43, CP43 polypeptide of PSII; CP47, CP47 polypeptide of PSII; D1, D1 polypeptide of PSII; D2, D2 polypeptide of PSII; DCBQ, 2,5-dichloro-*p*-benzoquinone; DCMU, 3-(3,4-dichlorophenyl)-1,1-dimethylurea; EPR, electron paramagnetic resonance; EXAFS, extended X-ray absorption fine structure; FTIR, Fourier transform infrared; OEC, oxygen-evolving complex; PSII, Photosystem II; XAS, X-ray absorption spectroscopy; Y_Z, tyrosine Z.

■ REFERENCES

(1) Umena, Y., Kawakami, K., Shen, J.-R., and Kamiya, N. (2011) Crystal structure of oxygen-evolving photosystem II at a resolution of 1.9 Å. *Nature 473*, 55−60.

(2) Kok, B., Forbush, B., and McGloin, M. (1970) Cooperation of charges in photosynthetic oxygen evolution. I. A linear four step mechanism. *Photochem. Photobiol. 11*, 457−475.

(3) McEvoy, J. P., and Brudvig, G. W. (2006) Water splitting chemistry of photosystem II. *Chem. Rev. 106*, 4455−4483.

(4) Pokhrel, R., McConnell, I. L., and Brudvig, G. W. (2011) Chloride regulation of enzyme turnover: Application to the role of chloride in photosystem II. *Biochemistry 50*, 2725−2734.

(5) Yocum, C. F. (2008) The calcium and chloride requirements of the O_2 evolving complex. *Coord. Chem. Rev. 252*, 296−305.

(6) Critchley, C. (1985) The role of chloride in photosystem II. *Biochim. Biophys. Acta 811*, 33−46.

(7) Lindberg, K., Vänngård, T., and Andréasson, L. E. (1993) Studies of the slowly exchanging chloride in photosystem II of higher plants. *Photosynth. Res. 38*, 401−408.

(8) Homann, P. H. (1988) Chloride relations of photosystem II membrane preparations depleted of, and resupplied with, their 17 and 23 kDa extrinsic polypeptides. *Photosynth. Res. 15*, 205−220.

(9) Lindberg, K., and Andréasson, L. E. (1996) A one-site, two-state model for the binding of anions in photosystem II. *Biochemistry 35*, 14259−14267.

(10) Kühne, H., Szalai, V. A., and Brudvig, G. W. (1999) Competitive binding of acetate and chloride in photosystem II. *Biochemistry 38*, 6604−6613.

(11) Bryson, D. I., Doctor, N., Johnson, R., Baranov, S., and Haddy, A. (2005) Characteristics of iodide activation and inhibition of oxygen evolution by photosystem II. *Biochemistry 44*, 7354−7360.

(12) Haddy, A., Hatchell, J. A., Kimel, R. A., and Thomas, R. (1999) Azide as a competitor of chloride in oxygen evolution by Photosystem II. *Biochemistry 38*, 6104−6110.

(13) Sandusky, P. O., and Yocum, C. F. (1986) The chloride requirement for photosynthetic oxygen evolution: Factors affecting nucleophilic displacement of chloride from the oxygen-evolving complex. *Biochim. Biophys. Acta 849*, 85−93.

(14) Sandusky, P. O., and Yocum, C. F. (1984) The chloride requirement for photosynthetic oxygen evolution. Analysis of the effects of chloride and other anions on amine inhibition of the oxygen-evolving complex. *Biochim. Biophys. Acta 766*, 603−611.

(15) Wincencjusz, H., Yocum, C. F., and van Gorkom, H. J. (1999) Activating anions that replace Cl^- in the O_2-evolving complex of photosystem II slow the kinetics of the terminal step in water oxidation and destabilize the S_2 and S_3 states. *Biochemistry 38*, 3719−3725.

(16) Wincencjusz, H., van Gorkom, H. J., and Yocum, C. F. (1997) The photosynthetic oxygen evolving complex requires chloride for its redox state $S_2 \rightarrow S_3$ and $S_3 \rightarrow S_0$ transitions but not for $S_0 \rightarrow S_1$ or $S_1 \rightarrow S_2$ transitions. *Biochemistry 36*, 3663−3670.

(17) Hasegawa, K., Kimura, Y., and Ono, T. A. (2002) Chloride cofactor in the photosynthetic oxygen-evolving complex studied by Fourier transform infrared spectroscopy. *Biochemistry 41*, 13839−13850.

(18) Ono, T., Zimmermann, J. L., Inoue, Y., and Rutherford, A. W. (1986) EPR evidence for a modified S-state transition in chloride-depleted photosystem II. *Biochim. Biophys. Acta 851*, 193−201.

(19) van Vliet, P., and Rutherford, A. W. (1996) Properties of the chloride-depleted oxygen-evolving complex of photosystem II studied by electron paramagnetic resonance. *Biochemistry 35*, 1829−1839.

(20) Beck, W. F., and Brudvig, G. W. (1986) Binding of amines to the O_2-evolving center of photosystem II. *Biochemistry 25*, 6479−6486.

(21) Haddy, A., Allen Kimel, R., and Thomas, R. (2000) Effects of azide on the S_2 state EPR signals from photosystem II. *Photosynth. Res. 63*, 35−45.

(22) Boussac, A., Ishida, N., Sugiura, M., and Rappaport, F. (2012) Probing the role of chloride in Photosystem II from *Thermosynechococcus elongatus* by exchanging chloride for iodide. *Biochim. Biophys. Acta 1817*, 802−810.

(23) Strickler, M. A., Walker, L. M., Hillier, W., and Debus, R. J. (2005) Evidence from biosynthetically incorporated strontium and FTIR difference spectroscopy that the C-terminus of the D1 polypeptide of photosystem II does not ligate calcium. *Biochemistry 44*, 8571−8577.

(24) Yachandra, V. K., Sauer, K., and Klein, M. P. (1996) Manganese cluster in photosynthesis: Where plants oxidize water to dioxygen. *Chem. Rev. 96*, 2927−2950.

(25) Vrettos, J. S., Limburg, J., and Brudvig, G. W. (2001) Mechanism of photosynthetic water oxidation: Combining biophysical studies of photosystem II with inorganic model chemistry. *Biochim. Biophys. Acta 1503*, 229−245.

(26) Hasegawa, K., Kimura, Y., and Ono, T. (2004) Oxidation of the Mn cluster induces structural changes of NO_3^- functionally bound to the Cl-site in the oxygen-evolving complex of photosystem II. *Biophys. J. 86*, 1042−1050.
(27) Boussac, A., and Rutherford, A. W. (1994) Electron transfer events in chloride-depleted photosystem II. *J. Biol. Chem. 269*, 12462−12467.
(28) McEvoy, J. P., and Brudvig, G. W. (2004) Structure-based mechanism of photosynthetic water oxidation. *Phys. Chem. Chem. Phys. 6*, 4754−4763.
(29) Olesen, K., and Andréasson, L. E. (2003) The function of the chloride ion in photosynthetic oxygen evolution. *Biochemistry 42*, 2025−2035.
(30) Haumann, M., Barra, M., Loja, P., Loescher, S., Krivanek, R., Grundmeier, A., Andréasson, L.-E., and Dau, H. (2006) Bromide does not bind to the Mn_4Ca complex in its S_1 state in Cl^--depleted and Br^--reconstituted oxygen-evolving photosystem II: Evidence from X-ray absorption spectroscopy at the Br K-edge. *Biochemistry 45*, 13101−13107.
(31) Murray, J. W., Maghlaoui, K., Joanna, K., Naoko, I., Lai, T.-L., Rutherford, A. W., Sugiura, M., Boussac, A., and Barber, J. (2008) X-ray crystallography identifies two chloride binding sites in the oxygen evolving centre of Photosystem II. *Energy Environ. Sci. 1*, 161−166.
(32) Guskov, A., Kern, J., Gabdulkhakov, A., Broser, M., Zouni, A., and Saenger, W. (2009) Cyanobacterial photosystem II at 2.9 Å resolution and the role of quinones, lipids, channels and chloride. *Nat. Struct. Mol. Biol. 16*, 334−342.
(33) Kawakami, K., Umena, Y., Kamiya, N., and Shen, J. R. (2009) Location of chloride and its possible functions in oxygen-evolving photosystem II revealed by X-ray crystallography. *Proc. Natl. Acad. Sci. U.S.A. 106*, 8567−8572.
(34) Rivalta, I., Amin, M., Luber, S., Vassiliev, S., Pokhrel, R., Umena, Y., Kawakami, K., Shen, J.-R., Kamiya, N., Bruce, D., Brudvig, G. W., Gunner, M. R., and Batista, V. S. (2011) Structural-functional role of chloride in photosystem II. *Biochemistry 50*, 6312−6315.
(35) Young, A., McChargue, M., Frankel, L. K., Bricker, T. M., and Putnam-Evans, C. (2002) Alterations of the oxygen-evolving apparatus induced by a 305Arg → 305Ser mutation in the CP43 protein of photosystem II from *Synechocystis* sp. PCC 6803 under chloride-limiting conditions. *Biochemistry 41*, 15747−15753.
(36) Bricker, T. M., Lowrance, J., Sutton, H., and Frankel, L. K. (2001) Alterations of the oxygen-evolving apparatus in a 448Arg → 448S mutant in the CP47 protein of photosystem II under normal and low chloride conditions. *Biochemistry 40*, 11483−11489.
(37) Putnam-Evans, C., and Bricker, T. M. (1997) Site-directed mutagenesis of the basic residues 321K to 321G in the CP 47 protein of photosystem II alters the chloride requirement for growth and oxygen-evolving activity in *Synechocystis* 6803. *Plant Mol. Biol. 34*, 455−463.
(38) Putnam-Evans, C., and Bricker, T. M. (1994) Site-directed mutagenesis of the CP47 protein of photosystem II: Alteration of the basic residue 448R to 448G prevents the assembly of functional photosystem II centers under chloride-limiting conditions. *Biochemistry 33*, 10770−10776.
(39) Clarke, S. M., and Eaton-Rye, J. J. (2000) Amino acid deletions in loop C of the chlorophyll *a*-binding protein CP47 alter the chloride requirement and/or prevent the assembly of photosystem II. *Plant Mol. Biol. 44*, 591−601.
(40) Clarke, S. M., and Eaton-Rye, J. J. (1999) Mutation of Phe-363 in the photosystem II protein CP47 impairs photoautotrophic growth, alters the chloride requirement, and prevents photosynthesis in the absence of either PSII-O or PSII-V in *Synechocystis* sp. PCC 6803. *Biochemistry 38*, 2707−2715.
(41) Tichy, M., and Vermaas, W. (1998) Functional analysis of combinatorial mutants altered in a conserved region in loop E of the CP47 protein in *Synechocystis* sp. PCC 6803. *Biochemistry 37*, 1523−1531.
(42) Faller, P., Rutherford, A. W., and Debus, R. J. (2002) Tyrosine D oxidation at cryogenic temperature in photosystem II. *Biochemistry 41*, 12914−12920.
(43) Debus, R. J., Campbell, K. A., Gregor, W., Li, Z.-L., Burnap, R. L., and Britt, R. D. (2001) Does histidine 332 of the D1 polypeptide ligate the manganese cluster in photosystem II? An electron spin echo envelope modulation study. *Biochemistry 40*, 3690−3699.
(44) Strickler, M. A., Walker, L. M., Hillier, W., Britt, R. D., and Debus, R. J. (2007) No evidence from FTIR difference spectroscopy that aspartate-342 of the D1 polypeptide ligates a Mn ion that undergoes oxidation during the S_0 to S_1, S_1 to S_2, or S_2 to S_3 transitions in photosystem II. *Biochemistry 46*, 3151−3160.
(45) Yamanari, T., Kimura, Y., Mizusawa, N., Ishii, A., and Ono, T. (2004) Mid- to low-frequency Fourier transform infrared spectra of S-state cycle for photosynthetic water oxidation in *Synechocystis* sp. PCC 6803. *Biochemistry 43*, 7479−7490.
(46) Service, R. J., Yano, J., McConnell, I., Hwang, H.-J., Niks, D., Hille, R., Wydrzynski, T., Burnap, R. L., Hillier, W., and Debus, R. J. (2011) Participation of glutamate-354 of the CP43 polypeptide in the ligation of manganese and the binding of substrate water in photosystem II. *Biochemistry 50*, 63−81.
(47) Chu, H.-A., Nguyen, A. P., and Debus, R. J. (1994) Site-directed photosystem II mutants with perturbed oxygen-evolving properties. 1. Instability or inefficient assembly of the manganese cluster in vivo. *Biochemistry 33*, 6137−6149.
(48) Kashino, Y., Koike, H., and Satoh, K. (2001) An improved sodium dodecyl sulfate-polyacrylamide gel electrophoresis system for the analysis of membrane protein complexes. *Electrophoresis 22*, 1004−1007.
(49) Kitagawa, N., Mazon, H., Heck, A. J. R., and Wilkens, S. (2008) Stoichiometry of the peripheral stalk subunits E and G of yeast V1-ATPase determined by mass spectrometry. *J. Biol. Chem. 283*, 3329−3337.
(50) Kashino, Y., Lauber, W. M., Carroll, J. A., Wang, Q., Whitmarsh, J., Satoh, K., and Pakrasi, H. B. (2002) Proteomic analysis of a highly active photosystem II preparation from the cyanobacterium *Synechocystis* sp. PCC 6803 reveals the presence of novel polypeptides. *Biochemistry 41*, 8004−8012.
(51) Roose, J. L., Kashino, Y., and Pakrasi, H. B. (2007) The PsbQ protein defines cyanobacterial photosystem II complexes with highest activity and stability. *Proc. Natl. Acad. Sci. U.S.A. 104*, 2548−2553.
(52) Shen, J. R., and Inoue, Y. (1993) Binding and functional properties of two new extrinsic components, cytochrome *c*-550 and a 12-kDa protein, in cyanobacterial photosystem II. *Biochemistry 32*, 1825−1832.
(53) Debus, R. J., Strickler, M. A., Walker, L. M., and Hillier, W. (2005) No evidence from FTIR difference spectroscopy that aspartate-170 of the D1 polypeptide ligates a manganese ion that undergoes oxidation during the S_0 to S_1, S_1 to S_2, or S_2 to S_3 transitions in photosystem II. *Biochemistry 44*, 1367−1374.
(54) Strickler, M. A., Hillier, W., and Debus, R. J. (2006) No evidence from FTIR difference spectroscopy that glutamate-189 of the D1 polypeptide ligates a Mn ion that undergoes oxidation during the S_0 to S_1, S_1 to S_2, or S_2 to S_3transitions in photosystem II. *Biochemistry 45*, 8801−8811.
(55) Noguchi, T., and Sugiura, M. (2002) Flash-induced FTIR difference spectra of the water oxidizing complex in moderately hydrated photosystem II core films: Effect of hydration extent on S-state transitions. *Biochemistry 41*, 2322−2330.
(56) Tommos, C., Madsen, C., Styring, S., and Vermaas, W. (1994) Point-mutations affecting the properties of $tyrosine_D$ in photosystem II. Characterization by isotopic labeling and spectral simulation. *Biochemistry 33*, 11805−11813.
(57) Suzuki, H., Kobayashi, T., Nakanishi, H., Nixon, P. J., and Noguchi, T. (2013) Functional roles of D2-Lys317 and the interacting chloride ion in the water oxidation reaction of photosystem II as revealed by Fourier transform infrared analysis. *Biochemistry*, DOI: 10.1021/bi301699h, in press.

(58) Chu, H. A., Hillier, W., Law, N. A., and Babcock, G. T. (2001) Vibrational spectroscopy of the oxygen-evolving complex and of manganese model compounds. *Biochim. Biophys. Acta 1503*, 69−82.
(59) Noguchi, T., and Berthomieu, C. (2005) Molecular analysis by vibrational spectroscopy. In *Photosystem II: The Light-Driven Water:-Plastoquinone Oxidoreductase* (Wydrzynski, T., and Satoh, K., Eds.) pp 367−387, Springer, Dordrecht, The Netherlands.
(60) Noguchi, T. (2007) Light-induced FTIR difference spectroscopy as a powerful tool toward understanding the molecular mechanism of photosynthetic oxygen evolution. *Photosynth. Res. 91*, 59−69.
(61) Noguchi, T. (2008) Fourier transform infrared analysis of the photosynthetic oxygen-evolving center. *Coord. Chem. Rev. 252*, 336−346.
(62) Service, R. J., Hillier, W., and Debus, R. J. (2010) Evidence from FTIR difference spectroscopy of an extensive network of hydrogen bonds near the oxygen-evolving Mn_4Ca cluster of photosystem II involving D1-Glu65, D2-Glu312, and D1-Glu329. *Biochemistry 49*, 6655−6669.
(63) Berthomieu, C., Hienerwadel, R., Boussac, A., Breton, J., and Diner, B. A. (1998) Hydrogen bonding of redox-active tyrosine Z of photosystem II probed by FTIR difference spectroscopy. *Biochemistry 37*, 10547−10554.
(64) Barth, A. (2001) The infrared absorption of amino acid side chains. *Prog. Biophys. Mol. Biol. 74*, 141−173.
(65) Noguchi, T., Ono, T.-a., and Inoue, Y. (1995) Direct detection of a carboxylate bridge between Mn and Ca^{2+} in the photosynthetic oxygen-evolving center by means of Fourier transform infrared spectroscopy. *Biochim. Biophys. Acta 1228*, 189−200.
(66) Noguchi, T., and Sugiura, M. (2003) Analysis of flash-induced FTIR difference spectra of the S-state cycle in the photosynthetic water-oxidizing complex by uniform ^{15}N and ^{13}C isotope labeling. *Biochemistry 42*, 6035−6042.
(67) Kimura, Y., Mizusawa, N., Ishii, A., Yamanari, T., and Ono, T. (2003) Changes of low-frequency vibrational modes induced by universal ^{15}N- and ^{13}C-isotope labeling in S_2/S_1 FTIR difference spectrum of oxygen-evolving complex. *Biochemistry 42*, 13170−13177.
(68) Noguchi, T., Sugiura, M., and Inoue, Y. (1999) FTIR studies on the amino-acid ligands of the photosynthetic oxygen-evolving Mn-cluster. In *Fourier Transform Spectroscopy: Twelfth International Conference* (Itoh, K., and Tasumi, M., Eds.) pp 459−460, Waseda University Press, Tokyo.
(69) Haumann, M., Liebisch, P., Mueller, C., Barra, M., Grabolle, M., and Dau, H. (2005) Photosynthetic O_2 formation tracked by time-resolved X-ray experiments. *Science 310*, 1019−1021.
(70) Gerencser, L., and Dau, H. (2010) Water oxidation by Photosystem II: H_2O-D_2O exchange and the influence of pH support formation of an intermediate by removal of a proton before dioxygen creation. *Biochemistry 49*, 10098−10106.
(71) Dilbeck, P. L., Hwang, H. J., Zaharieva, I., Gerencser, L., Dau, H., and Burnap, R. L. (2012) The D1-D61N mutation in *Synechocystis sp.* PCC 6803 allows the observation of pH-sensitive intermediates in the formation and release of O_2 from photosystem II. *Biochemistry 51*, 1079−1091.
(72) Clausen, J., Debus, R. J., and Junge, W. (2004) Time-resolved oxygen production by PSII: Chasing chemical intermediates. *Biochim. Biophys. Acta 1655*, 184−194.
(73) Hundelt, M., Hays, A.-M. A., Debus, R. J., and Junge, W. (1998) Oxygenic photosystem II: The mutation D1-D61N in *Synechocystis* sp. PCC 6803 retards S-state transitions without affecting electron transfer from Y_Z to P_{680}^+. *Biochemistry 37*, 14450−14456.
(74) Hwang, H. J., Dilbeck, P., Debus, R. J., and Burnap, R. L. (2007) Mutation of arginine 357 of the CP43 protein of photosystem II severely impairs the catalytic S-state cycle of the H_2O oxidation complex. *Biochemistry 46*, 11987−11997.
(75) Numao, S., Maurus, R., Sidhu, G., Wang, Y., Overall, C. M., Brayer, G. D., and Withers, S. G. (2002) Probing the role of the chloride ion in the mechanism of human pancreatic α-amylase. *Biochemistry 41*, 215−225.
(76) Liu, X., Fernandez, M., Wouters, M., Heyberger, S., and Husain, A. (2001) Arg1098 is critical for the chloride dependence of human angiotensin I-converting enzyme C-domain catalytic activity. *J. Biol. Chem. 276*, 33518−33525.
(77) Brayer, G. D., Luo, Y., and Withers, S. G. (1995) The structure of human pancreatic α-amylase at 1.8 Å resolution and comparisons with related enzymes. *Protein Sci. 4*, 1730−1742.
(78) Qian, M., Haser, R., and Payan, F. (1993) Structure and molecular model refinement of pig pancreatic α-amylase at 2.1 Å resolution. *J. Mol. Biol. 231*, 785−799.
(79) Larson, S. B., Greenwood, A., Cascio, D., Day, J., and McPherson, A. (1994) Refined molecular structure of pig pancreatic α-amylase at 2.1 Å resolution. *J. Mol. Biol. 235*, 1560−1584.
(80) Feller, G., le Bussy, O., Houssier, C., and Gerday, C. (1996) Structural and functional aspects of chloride binding to *Alteromonas haloplanctis* α-amylase. *J. Biol. Chem. 271*, 23836−23841.
(81) Maurus, R., Begum, A., Kuo, H.-H., Racaza, A., Numao, S., Andersen, C., Tams, J. W., Vind, J., Overall, C. M., Withers, S. G., and Brayer, G. D. (2005) Structural and mechanistic studies of chloride induced activation of human pancreatic α-amylase. *Protein Sci. 14*, 743−755.
(82) Bondar, A.-N., and Dau, H. (2012) Extended protein/water H-bond networks in photosynthetic water oxidation. *Biochim. Biophys. Acta 1817*, 1177−1190.
(83) Noguchi, T., Suzuki, H., Tsuno, M., Sugiura, M., and Kato, C. (2012) Time-resolved infrared detection of the proton and protein dynamics during photosynthetic oxygen evolution. *Biochemistry 51*, 3205−3214.
(84) Paddock, M. L., Feher, G., and Okamura, M. Y. (2003) Proton transfer pathways and mechanism in bacterial reaction centers. *FEBS Lett. 555*, 45−50.